UCLouvain

epl

École polytechnique de Louvain

A digital tool at the service of organology

Validation of a photogrammetric approach

Author: **Philémon Beghin**
Supervisors: **Anne-Emmanuelle Ceulemans**, **Paul Fisette**, **François Glineur**
Reader: **Vincent Wertz**
Academic year 2020–2021
Master [120] in Mathematical Engineering

Abstract

The morphology of today's violin differs greatly from that of the first instruments of the late 16th century. Indeed, in order to meet the standards suggested by famous orchestras and conservatories, many ancient violins have been recut. It is important for musicologists and organologists to analyse the alterations they have undergone. Specialists agree that the instruments have been reshaped, but have difficulty to prove it rigorously. Moreover, the historical testimonies about this process are imprecise. It is therefore necessary to find an objective way to quantify violin geometry. Hence, we have developed an IT tool that allows to locate the minima and inflection points relatively well on a violin body and to identify the shape of its contour lines. These analyses enabled to differentiate an ancient recut violin from an ancient non recut violin. We have also established the correspondence between a photogrammetric approach and a CT scan approach.

Acknowledgements

I would like first to sincerely thank my supervisors, Prof. Anne-Emmanuelle Ceulemans, Prof. Paul Fisette and Prof. François Glineur. In spite of the particular context that marked this academic year, their availability and their continuous support allowed me to carry out this research. The plurality between engineers and musicologist in our team offered us an interesting and enriching work dynamic from all points of view. Through our discussions, we identified the organological issues of this thesis and found the mathematical tools that would allow us to address the problems posed.

Of course, all this work would not have been possible without the excellent pictures taken by Iona Thys. Her contribution has certainly been essential to the results of our analysis. Although we did not have the opportunity to meet, I am truly grateful to her. I would like to take this opportunity to thank once again Mrs. Ceulemans, who was the intermediary between us.

Finally, I would like to thank my family for their support throughout this thesis. Their positive feedback and the value of hard work they have passed me on have always permitted me to go forward and to achieve my objectives.

Contents

Abstract **i**

Acknowledgements **iii**

Introduction **1**

1 Impact of reshaping on morphology **3**
1.1 Violin morphology . . . 3
1.2 Observable elements due to standardisation . . . 4
1.2.1 Re-cutting of the top and bottom of the sound box . . . 5
1.2.2 Removal of a slice of wood from the sound board or back . . . 7
1.3 Objectives . . . 7

2 State of the art **9**
2.1 A first approach: photogrammetry . . . 9
2.2 A second approach: medical CT scanners . . . 11

3 Data acquisition **15**
3.1 A first amateur shooting . . . 15
3.2 A professional shooting . . . 17

4 Fitting and minimisation problem **21**
4.1 Processing of the photogrammetric mesh . . . 21
4.1.1 Cleaning and repairing . . . 21
4.1.2 Orientation . . . 22
4.2 Mesh creation from the DICOM files . . . 26
4.3 Fitting of the two meshes . . . 29
4.3.1 Modelling of the matching problem . . . 29
4.3.2 Problem solving . . . 30

5 Characteristic points study **37**
5.1 Cutting through the mesh . . . 37
5.1.1 Mesh simplification . . . 37
5.1.2 Sound board and back separation . . . 38
5.1.3 Violin edges delimitation . . . 40
5.1.4 Planar sections through the mesh . . . 43
5.1.5 Sound board or back identification . . . 44
5.2 Location of the minima channel . . . 45
5.3 Location of the inflection points path . . . 49
5.4 Contour lines study . . . 51

6 Results **53**
6.1 Cuypers' viola . . . 54
6.1.1 Channel . . . 54
6.1.2 Inflection points path . . . 55
6.1.3 Contour lines . . . 55
6.2 Hofmans' viola . . . 56
6.2.1 Channel . . . 56
6.2.2 Inflection points path . . . 57
6.2.3 Contour lines . . . 58
6.3 3D visualisation . . . 59
6.4 Comparison between recut and non recut instruments . . . 60

Conclusion **63**

References **65**

Figures references **67**

List of figures **71**

Introduction

The violin as we know it today first appeared in Italy in the late 16th century [1]. The sound and tone of this instrument immediately became popular and the violin was exported throughout Europe. Luthiers continued to experiment and think about how to improve their instruments and making them more efficient. This wave of innovation gave birth to a very diverse family of violins for over 200 years. We had to wait until the 18th century to consider a standardisation of the different sizes of the instrument and until the 19th to make it definitive, thanks in particular to conservatories and renowned orchestras.

Nowadays, three types of violins can be distinguished according to their size: the violin itself, which is the smallest, the viola and the cello, the largest. Nevertheless, before standardisation, the size and the morphology of violins differed according to time and place. This is why, from 1750 onwards, ancient instruments had to be reshaped to fit new organological standards. In particular, there has been an important change in the violin bodies, which have been mainly preserved during the centuries. In view of the adoption of the new dimensions during the 19th century, many instruments were recut to a smaller size to match the new standardisation. Figure 1 shows the illustration of an inherited violin from the first half of the 18th century and an estimation of its original dimensions.



FIG. 1 – *Recut violin and estimation of its original dimensions. Height of the sound box: now* 35.4 *cm - original c.* 38 *cm*

A common issue for today's musicologists, organologists and luthiers is to determine whether an early violin has been recut and, if so, to quantify the alterations it has undergone. Specialists agree that the instruments have been reshaped, but have difficulty

to prove it rigorously. Moreover, the historical testimonies about this process are imprecise. It is therefore necessary to find an objective way to analyse violins. Some studies on the topic have already been carried out, notably two master theses written at the Ecole Polytechnique de Louvain (UCLouvain, Louvain-la-Neuve) [10][11]. Indeed, Prof. A.-E. Ceulemans, co-supervisor of these theses and curator of the Musical Instruments Museum (MIM, Brussels), was interested in this desire to characterise the ancient instruments stored in the museum. Many violins of the collection were made in the former Low Countries (roughly speaking, today's Netherlands, Belgium and Luxembourg) before the years of standardisation. It is therefore really interesting for the MIM to determine whether the dimensions of their instruments are genuine from that period or whether they have been altered.

The first thesis mentioned above used a photogrammetric approach, which consisted in taking pictures of the instruments and digitally reconstructing them in three dimensions using appropriate software. The second one raised the level of accuracy by using a medical CT scanner. The aim of this master thesis, the third on the subject, is also to develop an IT tool that could quantify the geometric singularities of ancient violins, but above all, to validate a come-back to the photogrammetric approach based on information from the scans.

We will conduct this research in the following manner. First, we will explicitly show the impact of reshaping on the morphology of violins in Chapter 1. Then, in Chapter 2, we will discuss the state of the art and the studies carried out in the two previous master theses. Afterwards, we will describe the data acquisition process and how to take good pictures in Chapter 3. Next, we will show in Chapter 4 how we linked the information of the scans to our acquisition. Chapter 5 is the most important. We will show how we handled the digital reconstruction of the violins and the underlying analysis of the characteristic points. Finally, we will present all the results in Chapter 6 and conclude whether the validation of the photogrammetric approach was successful or not.

Chapter 1

Impact of reshaping on morphology

1.1 Violin morphology

The violin is divided into three parts: the head, the neck and the body, also known as the sound box. The fingerboard, on which the musicians shorten the strings with the fingers of the left hand, is glued to the neck and then extends over the upper part of the sound box as we can see in Figure 1.1. In this thesis, we will focus on the body and thus, we need to show some of its elements before going further. The sound box is composed of several surfaces: the sound board, the back and lateral surfaces that connects them, called ribs. On the sound board, we can observe the F-holes which are used to diffuse the sound out of the sound box. There are 4 corners on each face of the body. The curvatures on the ribs, between two side corners, are called C-bouts. We could of course list many other elements of the violin's anatomy, but we will only mention these ones, visible in Figure 1.2, in the continuation of this work.

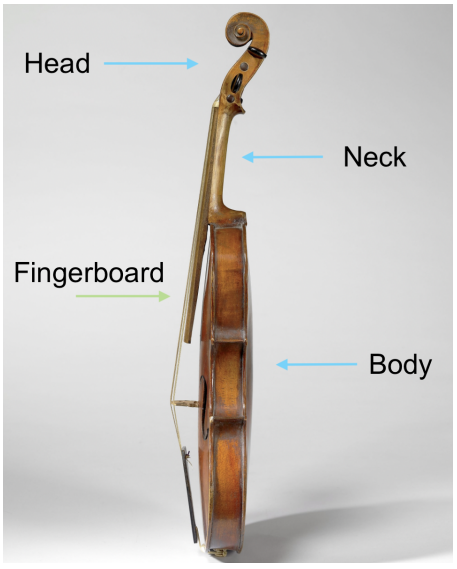


FIG. 1.1 – *Side view of the violin anatomy*

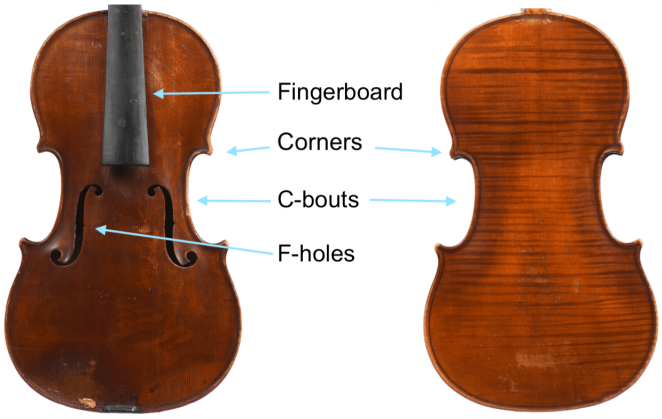


FIG. 1.2 – *Anatomy of the body, front view of the sound board (left) and back view (right)*

1.2 Observable elements due to standardisation

We can first mention that, in order to meet the new organological requirements of the late 18th and 19th centuries, the fingerboard and neck of ancient violins were replaced and tilted backwards to give more tension to the strings and thus a more powerful and clearer sound to the instrument. The difference between a baroque violin and a modern violin can be seen in Figure 1.3. To do this, the original neck was simply removed from the body and replaced with another, so that few of ancient necks have been preserved [5] [6] [7]. For this reason, we will not focus on this aspect in this master thesis.

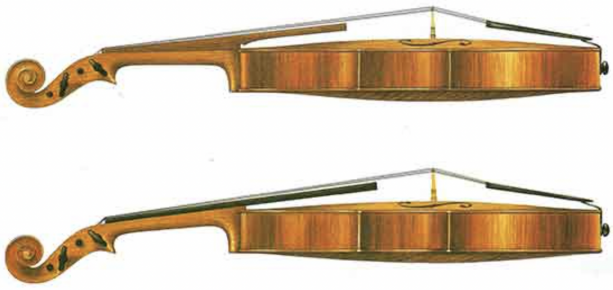
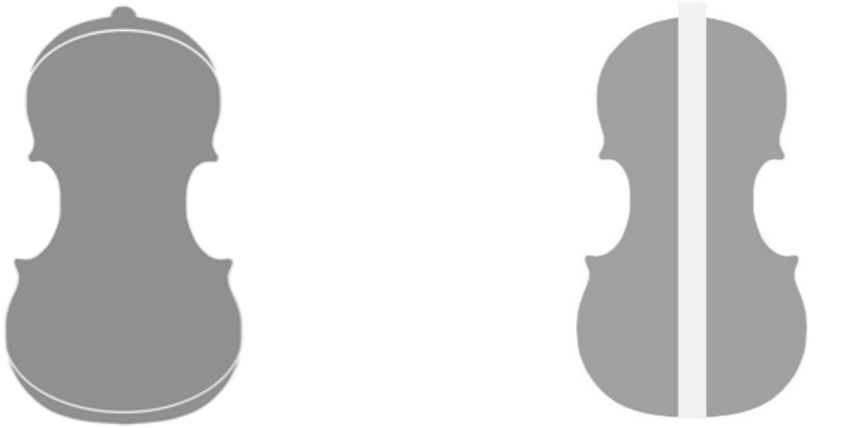


FIG. 1.3 – *Profile of a baroque violin (up) and a modern violin (down)*

However, as introduced above, most of the bodies were conserved over the centuries and we can therefore observe many transformations on them. We have already mentioned the re-cutting of the upper and lower parts of the sound box [3] [4]. Historical testimonies mention another type of re-cutting: the removal of a slice of wood in the axis of the sound board to reduce the width of the sound box [8] [9]. This second type of re-cutting was more likely practiced on larger instruments such as cellos, but the lack of evidence prevents us from reaching a definitive conclusion on this subject. We can discuss the impact of these two ways of reshaping on the present morphology and see what we can still observe today on ancient recut violins.



(a) *Top and bottom of the body*

(b) *Removal of a slice of wood*

FIG. 1.4 – *Different kinds of re-cutting*

1.2.1 Re-cutting of the top and bottom of the sound box

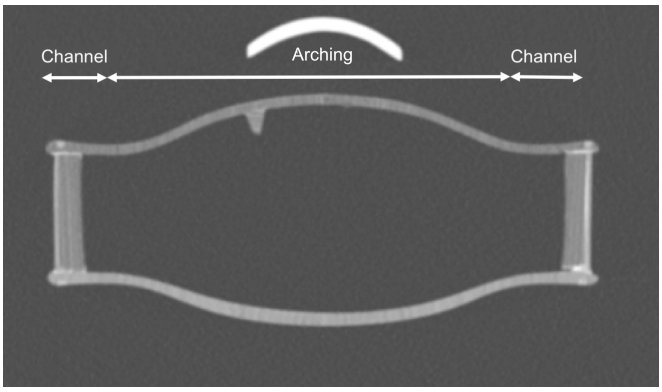
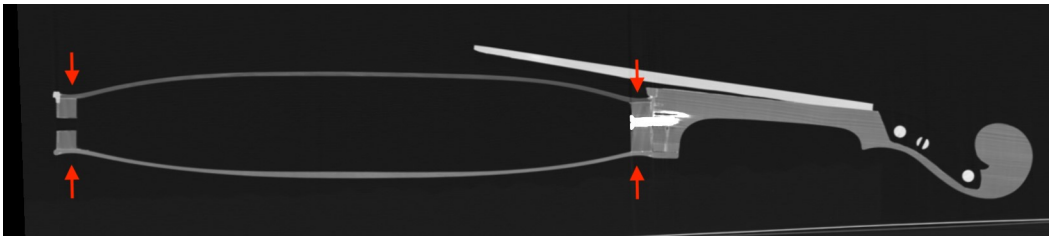


FIG. 1.5 – *Cross section of a violin*

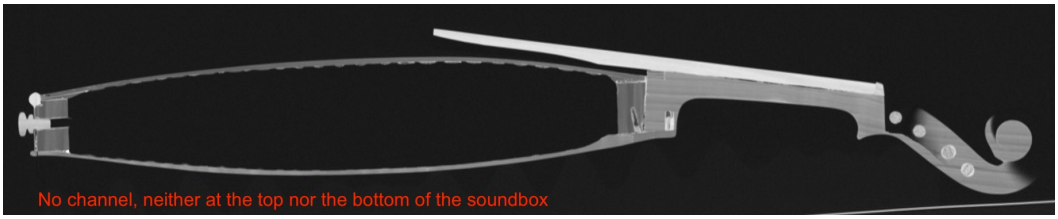
If we take a cross section of a violin, we can observe that the arching is surrounded by a channel on its left and right (both on the sound board and the back). This channel is in fact present all around the sound box. It can be clearly seen in Figure 1.6. When a violin is recut across the top and bottom of the sound box, this channel will tend to disappear near the ends and merge with the edges of the violin, as shown in Figure 1.7b. It is therefore essential to locate the channel precisely both on the sound board and on the back of the violin to get a first major indication of the potential reduction of the body.



FIG. 1.6 – *Channel on the violin sound board*



(a) *Non recut violin*



(b) *Recut violin*

FIG. 1.7 – *Sagittal section of a recut and non recut violin*

In the same way, we are also interested in the location of the inflection points all around the sound box, still on the sound board and on the back. They are located where the concavity of the soundboard or back changes. Figure 1.8 shows the inflection point (red) of a curve whose concavity differs from one side to the other. The inflection points path can also give some indication as to whether an instrument has been reshaped or not. It is also an important stylistic criterion, specific to each violin maker.

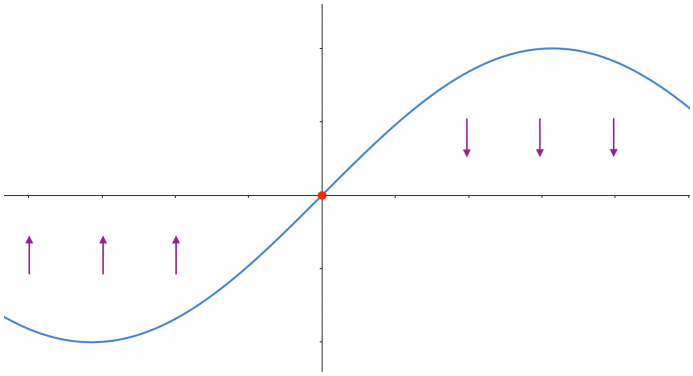
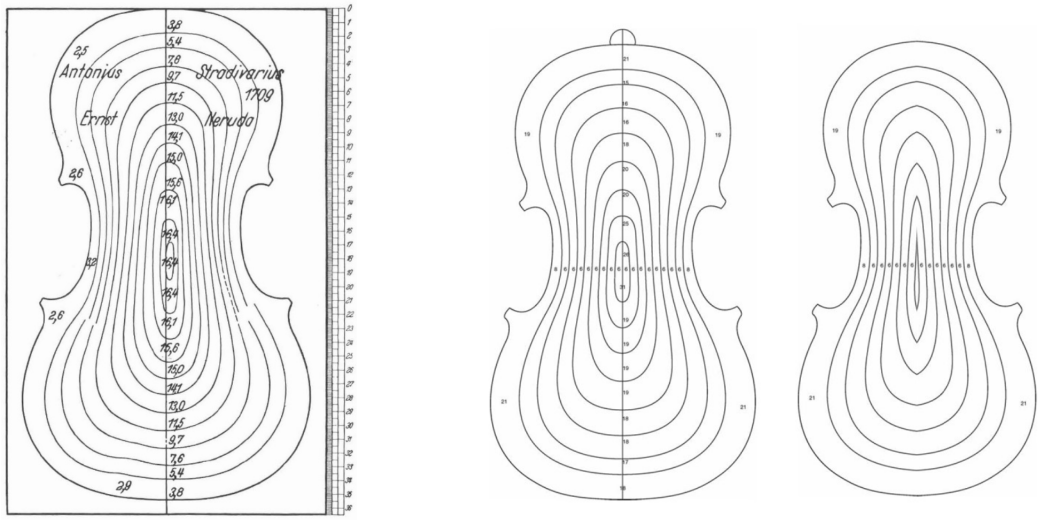


FIG. 1.8 – *Graphical representation of an inflection point (red)*

1.2.2 Removal of a slice of wood from the sound board or back

Luthiers rely on contour maps of violins in order to design the curvature of the body. Figure 1.9a shows a map based on a 1709 Stradivari violin. Even recut instruments were built in this way, although their original dimensions were quite loose and non-standard. Thus, by planing the sound board down the centre along the axis of the violin, the contour lines lose their smoothness and become much sharper. We can observe this effect directly in Figure 1.9b. In addition to studying the contour lines and their sharpness, we can again study the inflection points that may have been displaced due to the suppression of the slice of wood.



(a) *Luthier's map*

(b) *Before and after the slicing*

FIG. 1.9 – *Contour lines*

1.3 Objectives

As already mentioned, the aim of this thesis is to design a digital tool that could help to identify and quantify anomalies present on ancient violins and to determine whether they have been recut or not. Furthermore, we want to do this by validating a photogrammetric approach. The thesis based on CT scans [11] led to precise results, but for many reasons that we will discuss in the following chapter, the use of medical CT scanners is restrictive. We wanted to achieve a more accessible process, but without wasting the valuable information contained in the scans. Thus, we aim to reach an accuracy as close as possible to that of the scans but with an easier technique, photogrammetry.

In order to validate our results, we have chosen to work on two violins analysed by scans in the previous thesis. These two instruments, represented in Figures 1.10 and 1.11, are kept at the MIM. They were chosen in particular since they have provided good results in the past, and because only one of them has been recut. In this way, we will be able to show the distinction between a reshaped and a non reshaped instrument. Strictly speaking, both of them are violas (the intermediary violin size), but we will use the common name of violin throughout the thesis.



(a) *Frontal view of the sound board*



(b) *Profile view*

FIG. 1.10 – *Cuypers Johannes Theodorus, inv. no 2833, The Hague, 1761*



(a) *Frontal view of the sound board*



(b) *Profile view*

FIG. 1.11 – *Hofmans Matthys IV, inv. no 2846, Antwerp, before 1679*

The instrument of Hofmans, the oldest one, has been recut at some point in History, unlike Cuypers' which is much younger. For the sake of convenience, these violins will further be referred as:

- **Cuypers 2833**
- **Hofmans 2846**.

Chapter 2

State of the art

As instanced in the previous chapter, two theses on the same subject have already been completed. They used different techniques, respectively photogrammetry and medical imaging. We mentioned earlier that the CT scans approach was successful and gave good results. But how can we determine what is a good result and what is not ? This chapter will review the state of the art and answer these questions.

2.1 A first approach: photogrammetry

In 2017, the first thesis on violin geometry was written at UCLouvain by L. Motte [10]. The historical context and the desire to quantify the anomalies on ancient violins were already the same as here. However, there was no reference or previous work on this subject. How to design a digital tool to characterise violins ? A few processes have been considered to easily recreate an instrument in a numerical format. Medical scanners were suggested and mentioned in [10], but as it was a preliminary study, it was more practical to use a more accessible process. Photogrammetry was therefore chosen.

The main idea of photogrammetry is to create a mesh of an object from pictures. These pictures are processed by software that detects key points from one photo to the next. Hence, we need a lot of key points to be effective. Of course, the more pictures are taken, the more refined the mesh becomes. There are two main techniques for acquiring images: either the camera turns around the object to be reconstructed, or it is kept static and the object is rotated. In both cases, the rotation must be done gradually, from a few degrees to a few degrees. For her research, L. Motte chose to keep the camera static. This was probably the best idea for her thesis because she had no professional lighting and this technique allowed her to keep the light stable from one picture to the next. We can observe one of her pictures in Figure 2.1.



FIG. 2.1 – *Picture used by L. Motte to recreate the violin in 3D*

These photos were taken at 3 different heights and provided a reasonably good mesh with Autodesk ReCap (formerly Autodesk Remake)[1]. In order to distinguish the points of interest from the unnecessary elements, the background was removed to highlight the violin. However, one problem remained: the reflection on violin's varnish from the light in the room could not be removed. Because the reflections were omnipresent, it was really difficult to take sufficiently good pictures that would not damage the construction of the mesh. It was then important to minimise distracting light while taking pictures. Another issue concerned the support. Indeed, the pictures were only taken with a view of the sound board or the back, but never both, so that there is no way to reconstruct a complete violin mesh. This is not so problematic because the two surfaces were analysed separately, but it might prevent further analyses where the whole body of the violin is needed.

For a first attempt on the subject, it was difficult to estimate how to study the characteristic points on the mesh. Planar sections were suggested and this is indeed the more relevant way to proceed. But how to treat them ? In all three theses, we chose their direction from a 2D top view of the sound board or the back. L. Motte approximated the shape of the violins as follows:

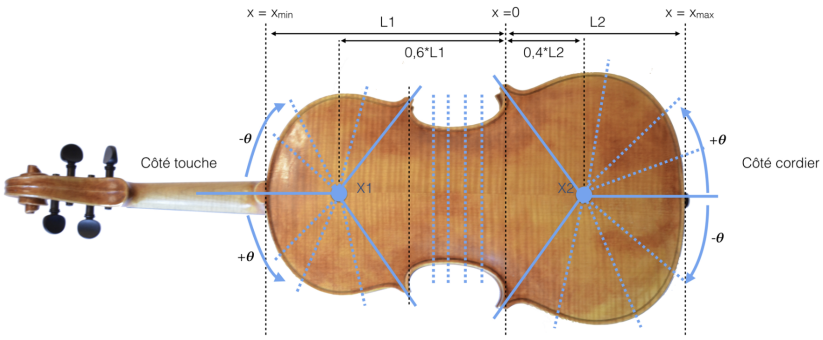
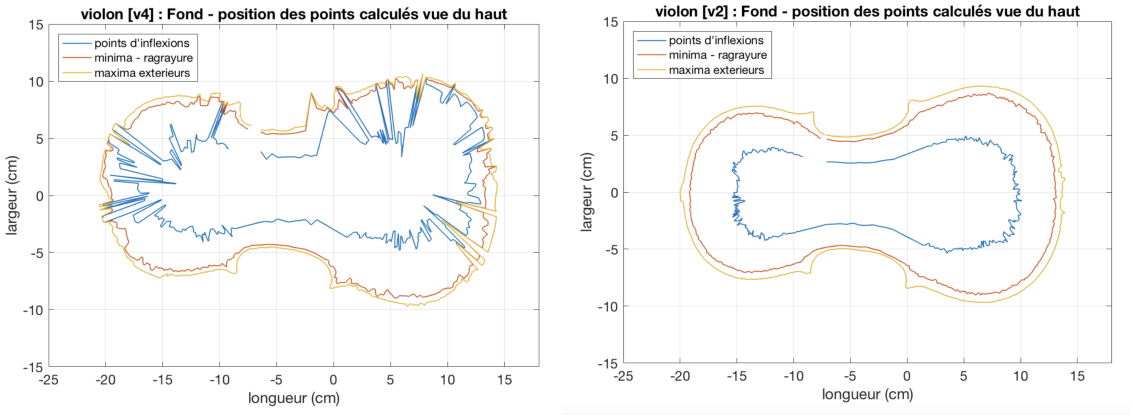


FIG. 2.2 – *Approximation of the violin sound board dimensions*

The planar cuts were performed every θ degrees according to the above dimensions for the left and right curved parts, and were orthogonal to the violin axis in the central part. The main drawbacks of this estimation are that the reference points were designed empirically, and especially that the same measurements were used on different instruments, which can be a source of inaccuracy. This first thesis ended with the results in Figure 2.3.

1. `https://www.autodesk.com/products/recap/overview?term=1-YEAR`

We can see the violin boundaries in yellow, the channel in orange and the inflection points path in blue. The graph in Figure 2.3a is the worst of all those provided. Some of them were actually representative and clear, as in Figure 2.3b, but the latter illustrates that the photogrammetric approach still lacked of precision.



(a) (b)

FIG. 2.3 – *Maps of two violin backs from [10]*

However, these results augured that we could be confident for the future, by rethinking the acquisition process and data processing, for example where and how to make the planar cuts. Nevertheless, we still have not answered an important question: what about the recut and non recut instruments ? The fact is that L. Motte did not have access to ancient violins and therefore only used recent ones, with the impossibility to comment on this aspect.

In conclusion, this first research proved that we could develop a digital tool to study the shape of violins. The results were not always clear, but this step had to be taken to be able to carry out advanced analyses. The lack of photographic equipment and the lack of similar studies did not help in the completion of that thesis, but the results motivated the supervisors to continue the research on the subject. Thus, we will see in the next section how R. Lothaire managed to deal with CT scans and ancient instruments, some of which have been recut.

2.2 A second approach: medical CT scanners

To compensate the lack or precision due to photogrammetry, CT scanners were used in R. Lothaire's thesis [11], as already suggested in [10]. He studied six instruments that had been scanned at the University Hospital of Saint-Luc (UCLouvain, Brussels-Woluwe). The numerical format of the scans is DICOM, which stands for *Digital imaging and communications in medicine*. The cross and sagittal sections represented in Figures 1.5 and 1.7 are DICOM images. The difficulty of dealing with DICOM files is much harder than that of dealing with photogrammetry. This is because the files do not contain any mesh or point cloud information, but simply grey scale images with different textures and densities. A DICOM file representing a viola contains about 2000 cross sections of 512×512 pixels, a huge number of squares to deal with. After a long filtering process, R. Lothaire finally obtained a set of black and white matrices, representing matter or empty space, which were much easier to process. Nevertheless, there was still an orientation problem to solve.

As the violin is a really complex body, it was difficult to place it straight on the scanner. It resulted in a tilted set of black and white matrices, such as the one shown in Figure 2.4.

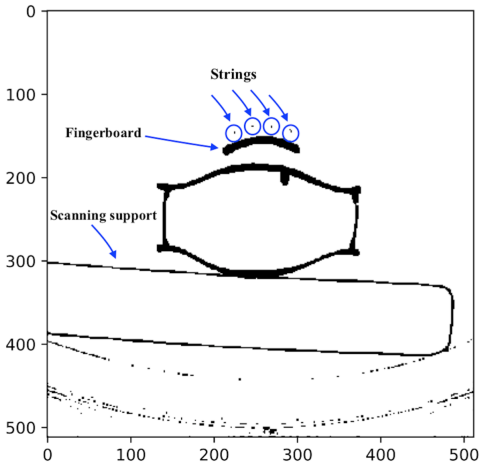
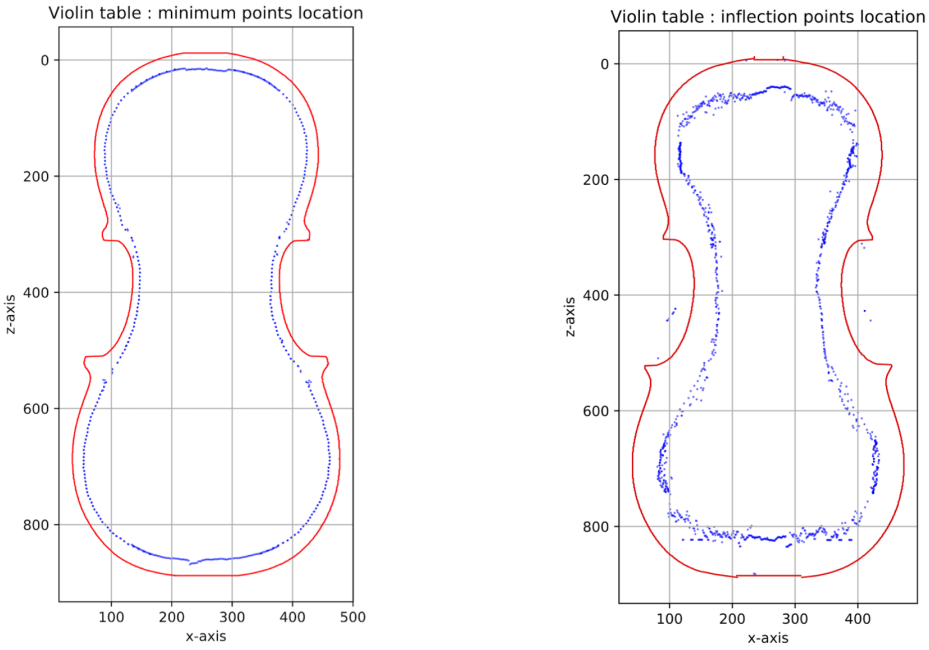


FIG. 2.4 – *Cross section of a matrix form violin*

The problem was solved in two ways: firstly, by coding a program that would refine the orientation and secondly, by printing a 3D support that would stabilise the violin in the scanner. Unfortunately, the second solution came too late to be validated: the new scans still contained some artefacts and it was too late in the semester to clean them up. However, they are still available. Eventually, R. Lothaire managed to process the rotated matrices and made some planar cuts to obtain relevant information. Figure 2.5 shows the results he obtained for the Cuypers 2833 sound board.



(a) *Minima channel*

(b) *Inflection points path*

FIG. 2.5 – *Minima channel and inflection points path on the Cuypers 2833 sound board*

We observe that the characteristic points have been located much more precisely than

those of the previous thesis. This is of course due to the accurate medical equipment, but also to a new way of making the planar cuts. The contour of the violin was approximated by a spline interpolation, and thus its derivative could be calculated everywhere. Then, it was straightforward to make the plane cuts perpendicular to the tangents as shown in Figure 2.6. This way of proceeding provided more accurate sections and finally more accurate characteristic points.

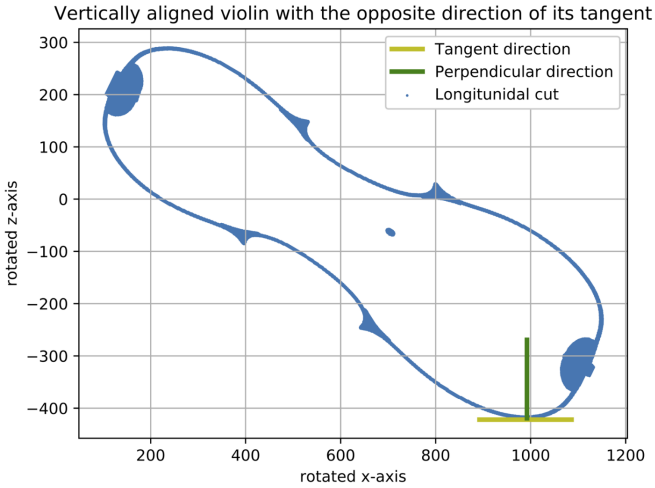


FIG. 2.6 – *New way of realising planar cuts, top view of a frontal cut*

We must mention that the axes scale of the graphs is a bit particular. Indeed, the units represent the transition between two consecutive slices of the DICOM files and not metric units. Thanks to the RadiAnt DICOM Viewer software[2], we can easily measure distances on the CT scans and know the number of calculated cross sections. We can therefore say that one 'DICOM unit' on the above graphs corresponds to approximately 0.45 mm.

Unfortunately, despite the good accuracy, the use of medical scanners is somehow restrictive. First, all the instruments brought from the museum to the hospital are historical works of art which need to be insured. Then, the amount of instruments that can be scanned is limited. Furthermore, the scanners themselves must remain available in case of emergency. It is difficult to find a slot for research when a patient's health may be at stake. Moreover, two technologists must be present. The first one adapts the scanner settings to the density and material of the violin wood and the second handles the scanner itself. Finally, some instruments carry pathogens and cannot be scanned. All those elements made us wonder if there was not a simpler way to proceed and we finally opted to go back to photogrammetry. Indeed, four years have passed since the first thesis and much progress has been made in this field. Thanks to the rise of 3D printing in recent years, 3D modelling software can handle many manipulations that will prevent us from tackling problems such as isolating the violin matter and rotation issues R. Lothaire had to face. Furthermore, we still have access to DICOM information, which will be helpful for this master thesis.

Thus, we can conclude this chapter by saying that thanks to the first photogrammetry thesis and the errors it involved, the second one led to some nice illustrations that we will try to match on this work. The ultimate goal of this third thesis is therefore to map

2. `https://www.radiantviewer.com/`

precisely the sound board and the back of the two violins, as in Figure 2.5, validating the return of the photogrammetric approach. To ensure continuity and consistency with the previous thesis, we will use Python[3] as programming language. The main advantages of Python are that it is widely used and completely free.

3. https://www.python.org/

Chapter 3

Data acquisition

In this chapter, we will explain how to take good pictures and to turn them into an accurate mesh. First, we tried to photograph the violins by ourselves directly at the museum and reconstruct them with Autodesk ReCap, which was used in [10]. We tried both of the proposed techniques for photogrammetry, i.e. turning the violin with a static camera and turning around it with the camera. Due to the simplicity of the equipment and the lighting, the reconstruction of the violins was limited. One of the techniques did not give any result and the second gave a few usable meshes, but not accurate enough to validate the results we wanted to recover. Finally, we were really lucky to collaborate with Iona Thys, photographer at the Royal Museums of Art and History (Brussels). She was already experienced in the field of photogrammetry through her involvement in various projects. Thanks to her, we obtained extremely precise meshes made with Agisoft Metashape[4], another photogrammetry software.

3.1 A first amateur shooting

We noted in Chapter 2 that we would prefer to have a mesh of complete violins and not just the sound board and the back separately. To do this, we photographed the violin suspended by its head, as in Figure 3.1a, by turning around it. We thought that the background elements of the pictures would help to detect the key points useful for matching, but the result was definitely worse. The software tried to generate furniture such as a frame or a shelf in place of the violin. As we had neither a suitable material nor a clean and good background, we abandoned this technique.

4. `https://www.agisoft.com/`



(a) *Suspended violin*



(b) *Lying violin*

FIG. 3.1 – *Two techniques of photogrammetry*

We then decided to return to the technique used by L. Motte, i.e. keeping the camera static and turning the lying violin. We tried to reduce the noise by putting a white tablecloth and focusing only on the instrument, as in Figure 3.1b. The drawback is that we revert to a different mesh for the sound board and the back. Figure 3.2 shows the simulated sound boards and backs for the two violins with Autodesk ReCap. We can notice that the sound boards are relatively well reconstructed, although there are still some flaws for the Cuypers 2833 (the twisted neck does not matter since we want to focus only on the body). On the other hand, the backs are completely distorted and therefore totally unusable. Cuypers 2833 back does not even represent a 3D object.



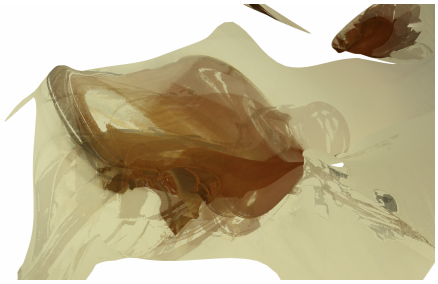
(a) *Hofmans 2846 sound board*



(b) *Cuypers 2833 sound board*



(c) *Hofmans 2846 back*



(d) *Cuypers 2833 back*

FIG. 3.2 – *Meshes obtained with Autodesk ReCap*

As we only had this material and no professional lighting to achieve the thesis, we

absolutely had to optimise our shooting to recreate the mesh. Sandie Le Conte[5], a former research engineer at the Musée de la Musique laboratory (Paris), suggested that we shoot around the static violin to reconstruct it, by adding targets surrounding the object. Printing the targets in Figure 3.3 on white sheets and placing them around the violin would help the software to focus on the key points. She also recommended to use Agisoft Metashape, but the license was not free. We were about to test the method she recommended, but fortunately, a discussion took place some times later with Iona Thys. After the talk, we knew we could base ourselves on her upcoming pictures and did not have to worry about the shooting anymore.

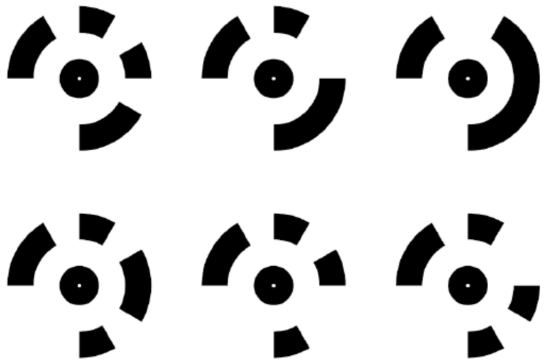


FIG. 3.3 – *Targets helping the reconstruction software*

3.2 A professional shooting

The precision we could reach with our resources was quite limited. In addition to that problem, as already mentioned, we would not be able to recreate one single mesh for the whole violin. As we had planned to compare the photogrammetric mesh and the DICOM files, this would have been a problem. Fortunately, thanks to Iona Thys, both issues of mesh quality and completeness were solved. Here is a brief explanation of what she did:

"In this project we applied photogrammetry. Photogrammetry is, in simple terms, the virtual reconstruction of an object from a series of photos. The two violins were placed on an automatic turntable. They were rotated through 360 degrees from different perspectives (heights). It is very important that the software that creates the 3D model receives enough information. The way the object is lit is also a very important aspect of the 3D process. We use a light tent for objects with a varnish layer, like the two violins. The light tent provides a very soft light and avoids strong reflections."[6]

Figure 1.6 already showed the aforementioned turntable. We can see in Figure 3.4 the light tent described by I. Thys.

5. `http://www.inp.fr/Recherche-colloques-et-editions/Recherche/Laboratoire-de-recherche/Equipe`

6. Free translation of her explanation from Dutch by A.-E. Ceulemans and Ph. Beghin.



FIG. 3.4 – *Light tent*

Both instruments were photographed[7] lying down on the turntable and upright on a wooden stick (always at different heights), as in Figures 1.6 and 3.4. Once all the pictures were taken, we could send them to a photogrammetry software. However, I. Thys wanted to raise the level of accuracy, so she eliminated the background of each picture via Photoshop[8], to highlight the mask of the violins. This procedure could be automated and it became very easy to obtain a large and nice set of pictures. Once each mask was ready, she sent them and the original pictures to Agisoft Metashape, formerly recommended by S. Le Conte. Indeed, I. Thys possessed a license that saved us from buying the software after the imprecise results returned by Autodesk ReCap. We could still have tried to send her pictures to Autodesk ReCap, but we preferred to let her work with her own equipment and her familiar way of proceeding.

Hence, the mask of each violin picture and the original images were sent to the software that finds the key points directly on the instruments. Each masked photo is also double-checked in case the masking procedure has failed and retained some artefacts. After finding the matching between the pictures, the software returns a sparse point cloud, true exoskeleton of the future complete mesh. Later on, the sparse point cloud is refined into a dense point cloud, which will create the final mesh. This last step is achieved by creating polygons between the appropriate points in the cloud. The model can now be exported to post-production software as ZBrush[9] which will perform finishing touches such as filling holes or removing faces that should not have been created. Finally a texture is applied to the mesh and our model is now completely ready. We can see the summarised process and the simulations of the two violins in Figures 3.5 and 3.6 respectively. The models are displayed in MeshLab[10], a 3D objects editing software.

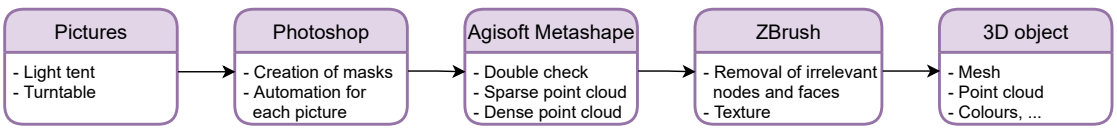


FIG. 3.5 – *Photogrammetric process*

7. The camera used was a Nikon D850 with a 60 *mm* focal length.
8. `https://www.photoshop.com/en`
9. `https://pixologic.com/`
10. `https://www.meshlab.net/`



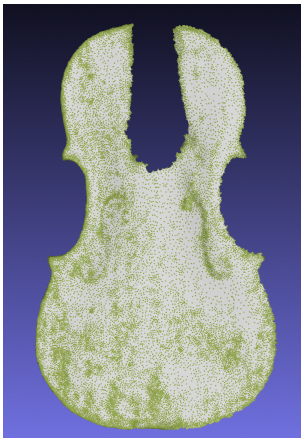
(a) *Cuypers 2833*



(b) *Hofmans 2846*

FIG. 3.6 – *3D models of both violins*

To convince ourselves that the reconstruction is much more accurate with this second attempt than with our first amateur one, we have compared the density of both point clouds of the Hofmans 2846 sound board, from which the fingerboard was removed. The points are in green and the faces of the mesh have been coloured in white to show the contrast between these geometric elements. We see directly in Figure 3.7 that the new point cloud is much more refined than the first one. We also note that during the re-creation process, Agisoft Metashape notices in the pictures that there is a depression at the F-holes, but interprets this only as a small hollow and not an actual hole in the violin. Thus, there is matter at this level of the mesh.



(a) *Amateur shooting*



(b) *Professional shooting*

FIG. 3.7 – *Comparison of the point clouds of the two shootings for the Hofmans 2846 sound board*

Should we compare the clouds, the first contains less than 20 000 nodes and the second more than 500 000. Taking the exact values, we obtain a density ratio of about 30. A really close surface ratio is obtained with the number of faces of each mesh.

In conclusion of this chapter, we can affirm that data acquisition and especially the way of taking pictures and processing them is really important in a photogrammetric procedure. With the right equipment and an efficient way of processing the images, one can increase the precision of the reconstructed violin by a factor 30, which is incredibly huge. Thanks to the work of Iona Thys, we will be able to perform accurate analyses. In addition, the availability of the whole modelled violin will be definitely useful for an important part of our validation approach in the next chapter. Indeed, we will show how close are the mesh constructed by I. Thys and the DICOM files. Figure 3.8 illustrates the complete process of this thesis with the different software used. It shows the intermediate steps we will take, from the pictures shooting until the 3D display of our results.

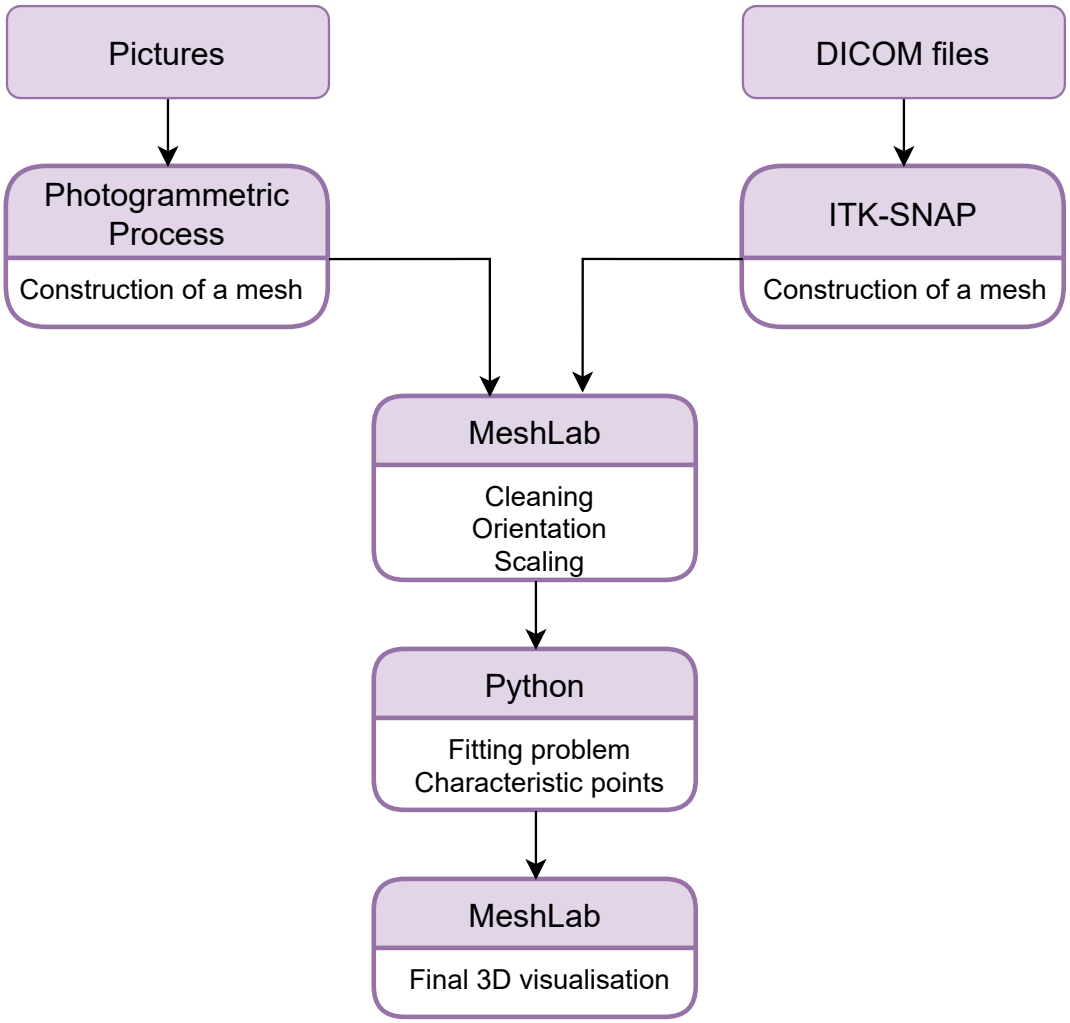


FIG. 3.8 – *General process of the thesis*

Chapter 4

Fitting and minimisation problem

We have already defined the main objective of this research, which is to recover results as precise as in [11] with a photogrammetric approach. We have shown in the previous chapter that we were able to recover an accurate mesh modelling the violins. The question we now ask ourselves is whether there is a matching between the mesh created by photogrammetry and the DICOM files used in the previous thesis. We will demonstrate that such a correspondence does indeed exist. First, we will show how the received mesh will be processed with sufficient precision (cleaning, scaling, orientation, ...). Then, we will explain what we have done to convert the DICOM files into another mesh in order to compare related 3D objects.

4.1 Processing of the photogrammetric mesh

4.1.1 Cleaning and repairing

The violins displayed in Figure 3.6 are visually convincing. However, they are not ready to be used directly. First, we note that starting for now, we will work only with the body of the violins as stated in Chapter 1, and we have therefore removed the neck from the mesh. Regarding the fingerboard hanging over the sound box, we could remove it from the Cuypers 2833 but not for the Hofmans 2846. Indeed, in the re-creation process, Agisoft made it distinct from the body in the first case, but in the second, the fingerboard has been merged with the body and therefore removing it would create a hole in the sound board. We can see the resulting violins in Figure 4.1.



(a) *Cuypers 2833* (b) *Hofmans 2846*

FIG. 4.1 – *Fingerboard distinct or merged with the body*

Unfortunately, the removal of Cuypers 2833 fingerboard was not optimal. We can see in Figure 4.2a that it left a few holes in the mesh. However, MeshLab has a surface reconstruction process and by specifying this small area to be refined, the software was able to recreate some points in the cloud as we can see in Figure 4.2b (the points are green highlighted). We see that the recreated points are not as dense as the original, but this will still prevent us from losing too much precision. We should note that having one violin with the fingerboard and one without will not be a problem. We will deal with this difference when recreating the DICOM meshes.



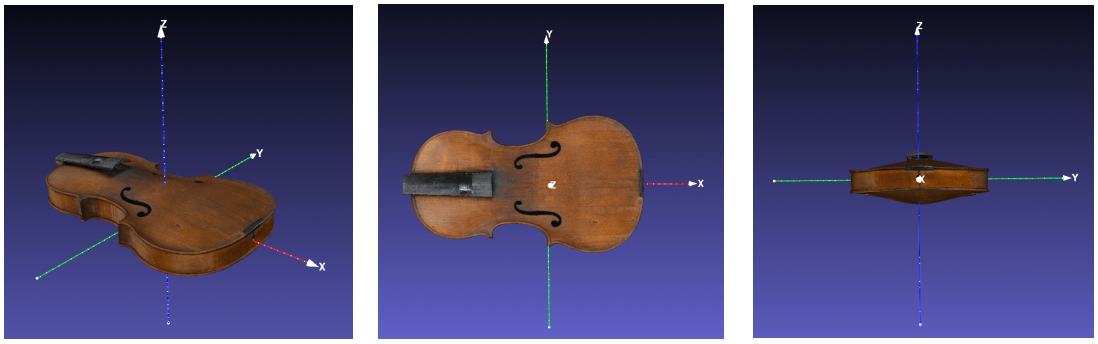
(a) *Before filling holes* (b) *After*

FIG. 4.2 – *Cuypers 2833 repair*

4.1.2 Orientation

We now need to define a frame for our digital representation. We have done this as in Figure 4.3, so that the x-axis is within the length of the sound board and the y-axis joins the two lower corners. Consequently, the z-axis is upwards. The origin is defined to be in the middle of the sound box. However, the received meshes are not expressed is this frame. We then have to translate and rotate them to do so. All these manipulations are available in MeshLab[11]. Nevertheless, it is really difficult to manually adjust the rotations and the translations with our frame perfectly.

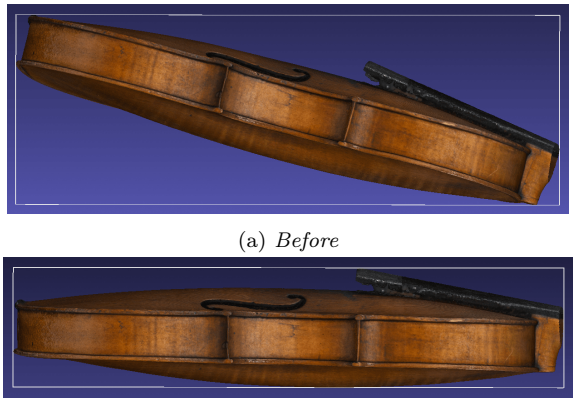
11. The documentation of the software is mainly done in the form of videos format. We would like to cite the Youtube channel of Mister P. MeshLab Tutorials in [14] for all the useful manipulations that we used in this work.



(a) *Perspective view* (b) *Orthogonal xy view* (c) *Orthogonal yz view*

FIG. 4.3 – *Different views of the reference frame*

The rotations and alignments from a violin to the other are extremely important. Indeed, as in [10] and [11], we will be working from a 2D top view of the violin to perform our planar cuts in 3D. How to ensure that this approach is reliable and will not lead to biased analysis ? To solve both issues (accuracy of the rotations and therefore the justification of the 2D approach), we will orientate our violins with the frame axes using Principal Component Analysis (PCA). This computationally efficient transformation is available in MeshLab, and we can therefore apply it easily. The PCA allows to determine the directions that best explain the dispersion of points in a cloud. In our case, the software considers 3 directions which correspond to the 3 directions of the space. MeshLab will therefore try to find the 3 orthogonal axes in the cloud that best represent the orientation of the violin. Figure 4.4 shows the instrument before and after the operation. The white frame is a 3D bounding box, whose edges are aligned with the frame axes. We see that the violin in Figure 4.4a is not aligned with the box, and therefore not with the axes either. However, after the PCA alignment, it is straight in the bounding box.



(a) *Before*

(b) *After*

FIG. 4.4 – *Before and after the PCA alignment*

The orientation of the mesh is now orthogonal to the axes, but not necessarily according to the reference directions we defined earlier, as in Figure 4.5. However, this will not be a problem. Indeed, we can apply right-angle rotations directly in MeshLab. This will preserve the principal components orientation and simply align the mesh with the axes we defined above.

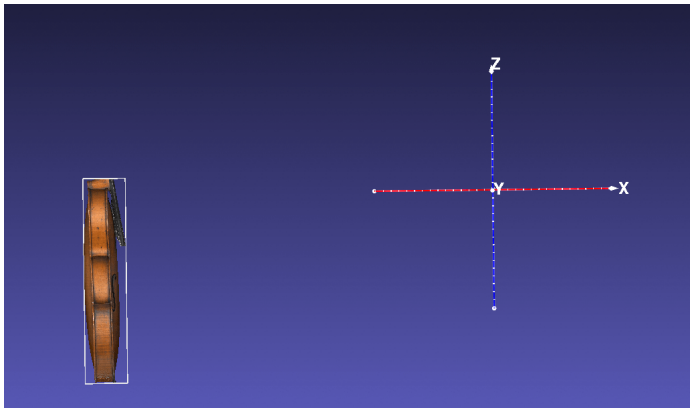
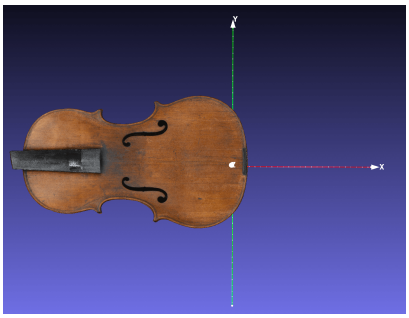
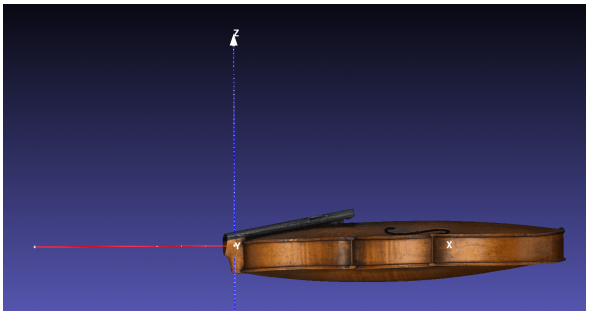


FIG. 4.5 – *Alignment of the bounding box and the frame after the PCA*

We still need to discuss translations. We have defined the origin as being in the middle of the sound box. Nevertheless, this notion is vague. In the same way as we asked ourselves earlier, how could we manually place the origin there perfectly ? We could set the middle of the bounding box on the axis, but because of the fingerboard (for the Hofmans 2846), the middle of the bounding box will not correspond to the middle of the sound box. This is not really a problem either. As we saw earlier, rotations and alignments are essential to perform a good analysis and justify the 2D approach of the cuts, but translations not so much. It is enough to impose that the mesh is sufficiently well placed according to the reference frame we described above (i.e. we tolerate an error of a few *mm* for the x and z axes regarding the notion of centre). Indeed, we are going to analyse the whole violin anyway. As the gradation of the axes is relative, shifting the analysis a few mm in either direction will not change the final results. In the same way, the position of the y axis is not that important either. It could have been placed in the centre of the C-bouts or aligned with the two upper corners, but we have arbitrarily chosen the two lower ones. For example, Figure 4.6 shows two other reference frames that we could have used, by translating the position of the y axis along the x axis.



(a) *Positive translation of the y axis, xy view*

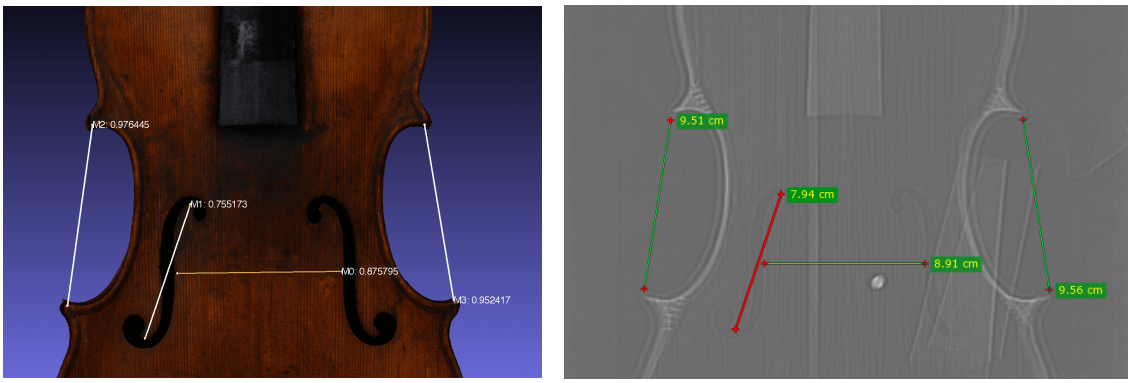


(b) *Negative translation of the y axis, xz view*

FIG. 4.6 – *Other possible reference frames by moving the y axis on the x axis*

Now the mesh is properly aligned, there is one last step to perform before it is fully useful: the scaling. When creating the model, Agisoft takes into account the relative measurements of the violin, but the software is unable to calculate the actual dimensions of the instruments. Fortunately, we can easily access them using DICOM files and RadiAnt Viewer. Therefore, we measured some typical distances on the instruments such as the difference between the corners or the F-holes, in both MeshLab and RadiAnt. These distances

were computed on an orthogonal view based on the alignment done in the previous subsection. An important assumption must be made to continue : the scanned measurements are considered true and reliable[12]. Once this assumption is made, we can then relate the measures on the scanned body and the photographed body as in Figure 4.7.



(a) *MeshLab* (b) *RadiAnt Viewer*

FIG. 4.7 – *Comparison of the measures in MeshLab and RadiAnt Viewer*

In order to keep a good precision, we chose to work throughout the thesis in mm[13]. Once the measurements have been made, we average all the scale ratios to find the final one which we will multiply the photogrammetric violin with. As this aspect ratio is obtained from an average, it inserts a first error term into the minimisation problem that will be presented later in this chapter.

Another remark has to be made about the colours of the violins. We can notice that the Hofmans 2846 is darker in Figure 4.7a than in Figure 3.6. Indeed, the file format of the simulations received by I. Thys is .obj, which is a standard in 3D modelling. Before having her models, we arbitrarily chose to work with another one, the .ply format. Most 3D formats have a lot in common, especially the basic information about the coordinates of the points of the cloud or the faces of the mesh. We can easily convert files from one to the other using online tools. As we only focused on the point cloud and the mesh, we did not specify any parameter for the colours, so the conversion automatically turned it darker. We will then work with the .ply format and omit the colours on the thesis.

This concluded the transformations made to the mesh provided by Agisoft. We have now an actual digital representation of the violin ready to be used. We will explain in the next section how we obtained a similar representation from the DICOM files, and then compare the two meshes.

12. After a discussion with Alain Vlassenbroek, physicist at Philips Healthcare who worked with the IQon Spectral IT scanner, we concluded that there is a priori no error in the measurements. The latter can be influenced by parameters (such as the pitch, the resolution, the cone beam effects, ...) and by the reconstruction technique but can be considered optimal. An important parameter to discuss is the number of slices per cm. A. Vlassenbroek told us that the maximum performance of the CT scanner is about 24 $slices/cm$ which corresponds approximately to one slice every 0.4 mm. We reported in Chapter 2 that the violins have been scanned about every 0.45 mm, which is very close to the optimal performance. We therefore conclude that the scans are optimal and representative of the actual measurements of the violins.

13. Contrary to [10] and [11] who worked in cm and slice indices (or 'DICOM discrete units').

4.2 Mesh creation from the DICOM files

Now our photogrammetric mesh is ready for comparison, we still need a 3D representation of the DICOM files. In order to compare similar objects and draw concrete conclusions, we decided to convert the medical images into a mesh. The ITK-SNAP software[14] can reconstruct meshes from scans, based on the contour segmentation algorithm detailed in [12]. Firstly, we need to set a viewing threshold to observe the scanned data in blue and white contrast, as in Figure 4.8. Once this is done, we need to add small red bubbles all over the different sections to create the mesh. The reconstruction algorithm is based on the propagation of the bubbles over the white areas of the sections. The more bubbles we have, the more accurate the final result will be. We set the size of the bubbles to be small in order to avoid swelling effect during the reconstruction. We can follow the 2D and 3D evolution of the process in Figures 4.9 and 4.10. We stop the reconstruction when the red bubbles have spread all over the blue and white sections. It may take some time to arrange the bubbles manually over all the sections, in order to cover a large number of areas. However, once this pre-processing task is done, the algorithm runs in a few minutes.

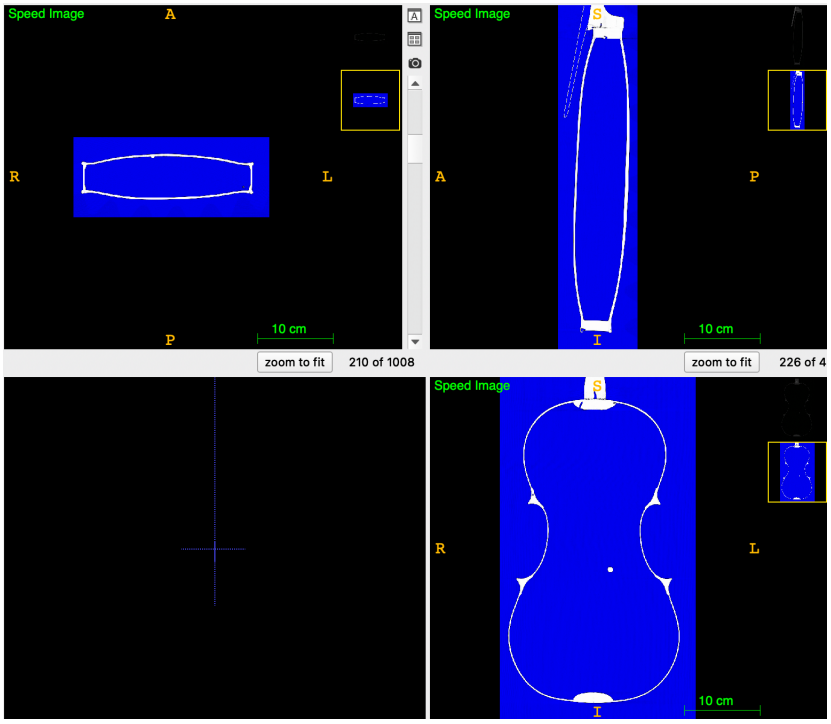
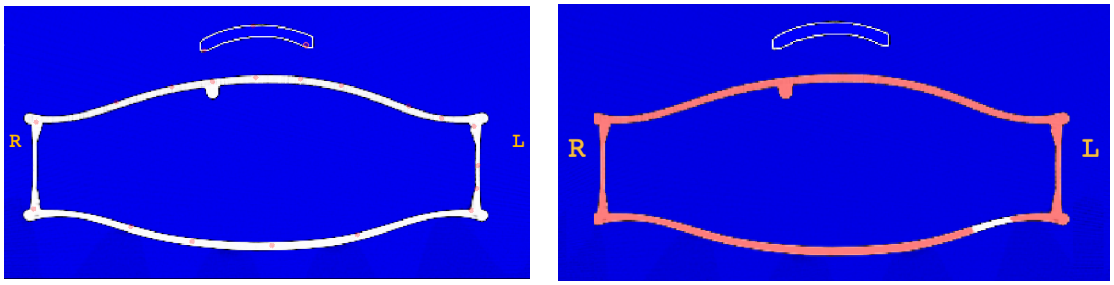


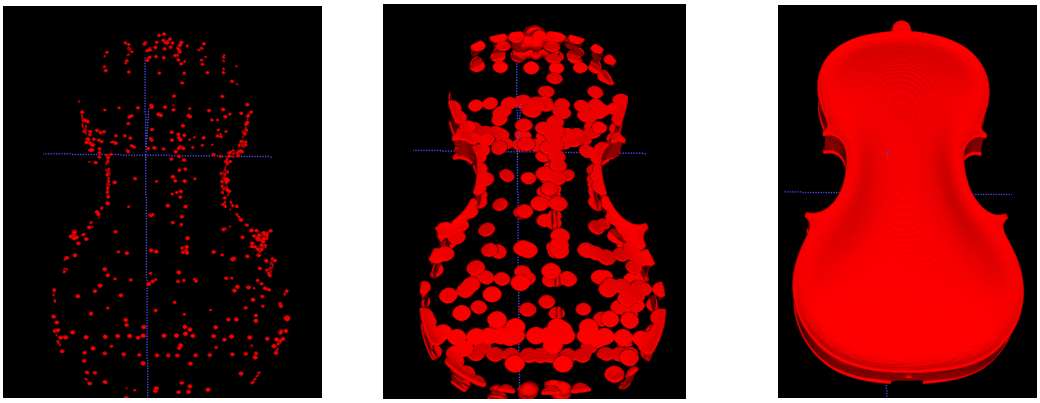
FIG. 4.8 – *Cuypers 2833 cross section (top left), sagittal section (top right) and frontal section (bottom right) in ITK-SNAP*

14. `http://www.itksnap.org/pmwiki/pmwiki.php`



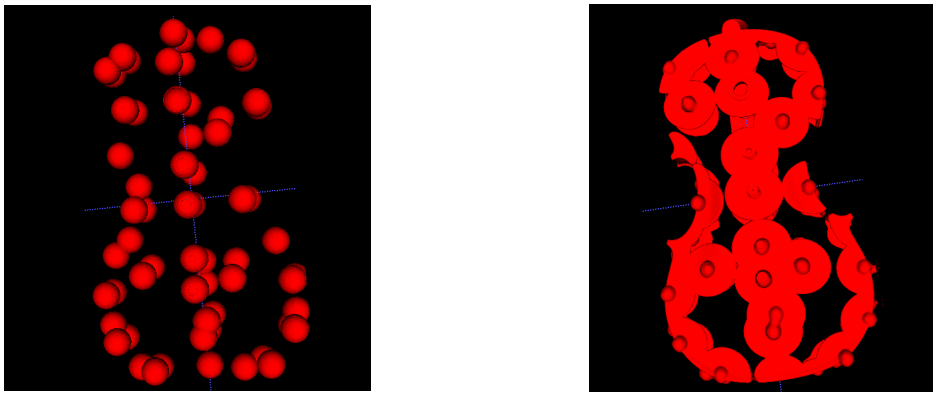
(a) *Initialisation of the algorithm* (b) *Iteration 200*

FIG. 4.9 – *2D evolution of the algorithm on cross sections*



(a) *Iteration 25* (b) *Iteration 100* (c) *Iteration 750*

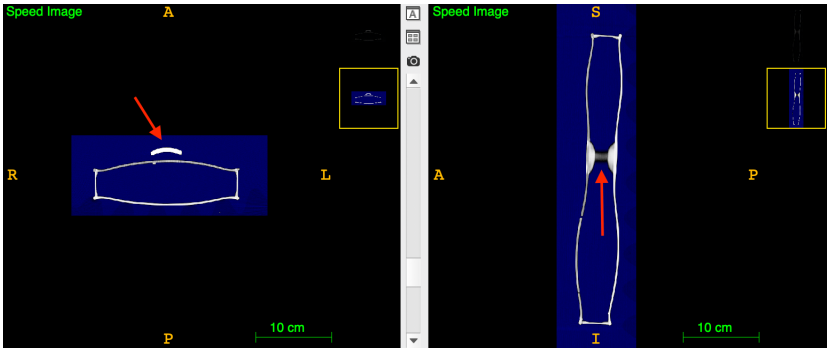
FIG. 4.10 – *3D evolution of the algorithm*



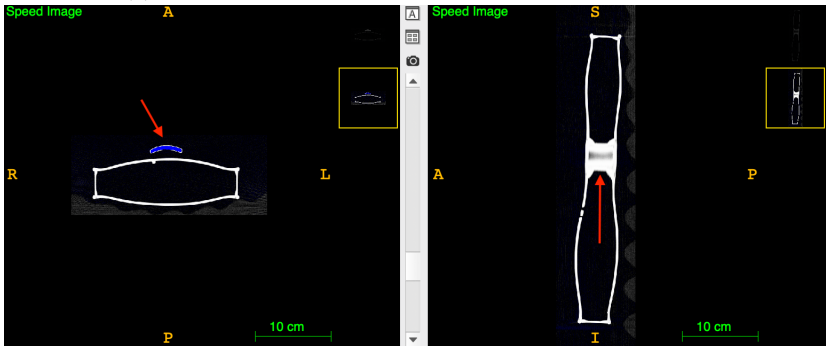
(a) *Initialisation with too big bubbles* (b) *Iteration 220*

FIG. 4.11 – *Swelling effect to be avoided*

The recreated DICOM meshes are even denser than the ones obtained by photogrammetry, which is promising as they are supposed to represent the actual measures of the violin. However, even if the DICOM files were considered ideal, the algorithm is very sensitive to the grey scale of the CT scans and sometimes cannot reconstruct all the details. Indeed, depending on the threshold set, it is really difficult to detect either the fingerboard or the cavity of the C-bouts. The difference can be seen in Figure 4.12. The red arrows show the fingerboard and the C-bout with different white intensities.



(a) *Threshold for a better reconstruction of the fingerboard*



(b) *Threshold for a better reconstruction of the cavity of C-bouts*

FIG. 4.12 – *Different thresholds*

Thus, we had to choose, for both violins, between keeping the fingerboard or a complete reconstruction of the ribs. We wanted to test both approaches for our matching problem (see section 4.3) and so, as we saw in Figure 4.1b that the Hofmans 2846 fingerboard was merged with the body, we focused on the fingerboard for this one and on the C-bouts for the Cuypers 2833. The reconstructed DICOM violins are shown in Figure 4.13. We can see at the top the Cuypers 2833 without the fingerboard and at the bottom the Hofmans 2846 with the fingerboard but with a few missing nodes in the C-bouts. Hence, even though we started with ideal medical files, converting them into a mesh introduced a new source of error.

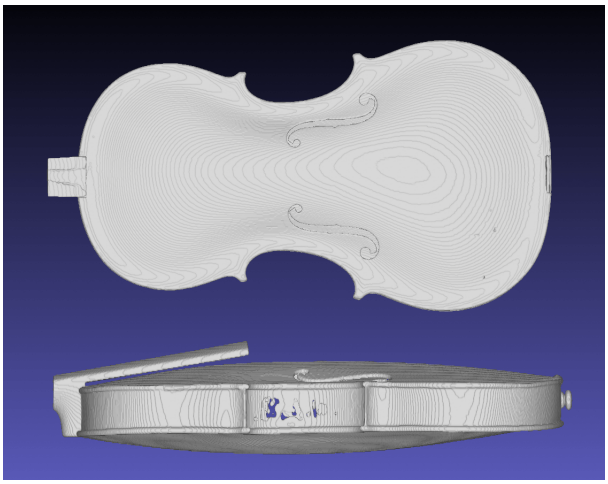


FIG. 4.13 – *DICOM meshes of Cuypers 2833 (top) and Hofmans 2846 (bottom)*

We must notice that the curved lines we can observe are not linked to contour lines but to an automatic texture process. Indeed, we will see in Chapter 5 that the contour lines do not resemble these curves at all.

4.3 Fitting of the two meshes

At this point, we have shown how we reconstructed two dense meshes for each violin, from photogrammetry and DICOM files. We now want to see how close they are in order to know if we can validate our photogrammetric approach. We mentioned that, unfortunately, some errors were induced during both reconstruction processes. However, we can balance them by saying that they concern only a few nodes out of the meshes composed of about 2 million points for the DICOM ones and 1,5 million for the photogrammetric ones. Therefore, we can still hope that the errors will not affect our correspondence analysis too much.

4.3.1 Modelling of the matching problem

We must now formalise the situation. Both meshes have coordinates expressed in the same frame of reference, assumed to be that of the scanned violin. In order to quantify the degree of similarity of these 3D representations, we would like to express the photographed violin in its own frame and see if its local coordinates in this frame are close to the scanned violin coordinates in the frame of reference. Thus, we have :

- A scanned violin V_{scan} expressed in the frame of reference $[\hat{R}^{VS}]$
- A photographed violin $V_{picture}$ expressed in the same reference $[\hat{R}^{VS}]$

We can see the graphical representation of the problem in Figure 4.14.

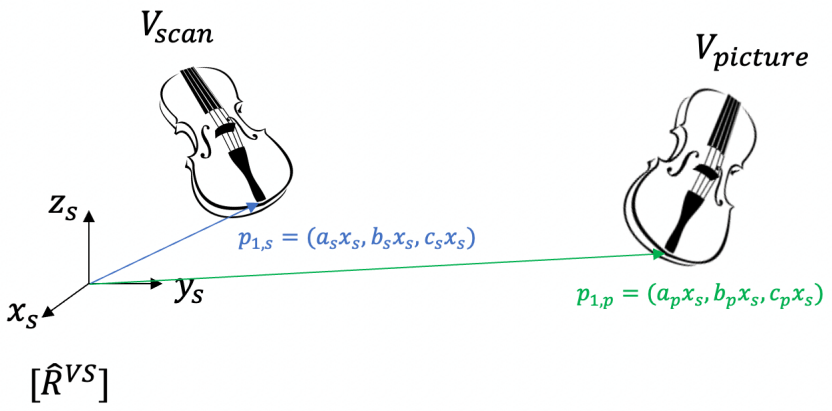


FIG. 4.14 – *Representation of both meshes in the frame of reference*

We need to find a new frame $[\hat{R}^{VP}]$ such that

$$V_{picture} \; in \; [\hat{R}^{VP}] \approx V_{scan} \; in \; [\hat{R}^{VS}]. \tag{4.1}$$

We will find it thanks to the 6 parameters X, Y, Z, θ_1, θ_2 and θ_3 corresponding to the elementary translations and rotations this new frame has to undergone to correspond to the reference frame. These transformations can be seen in Figure 4.15. The translation

vector is highlighted in purple and we can see the impact of the rotation on the new dashed axes.

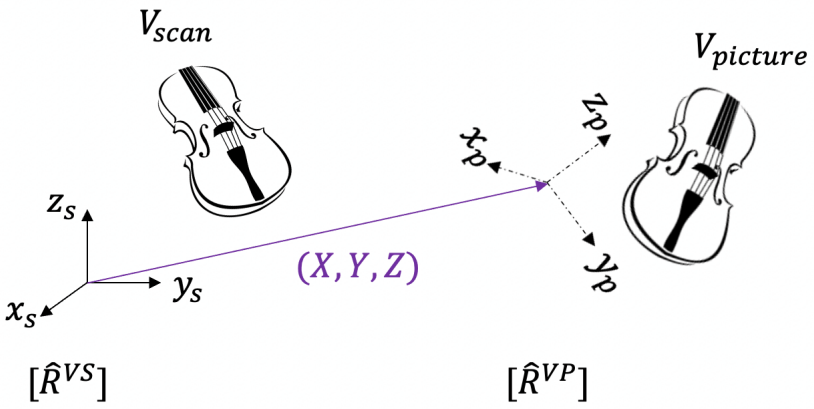


FIG. 4.15 – *Representation of both meshes in their own frame*

We can then rewrite Approximation 4.1 as

$$V_{picture} \approx R \cdot V_{scan} + \begin{pmatrix} X \\ Y \\ Z \end{pmatrix} \quad (both\ expressed\ in\ [\hat{R}^{VS}]) \tag{4.2}$$

with

$$R = \begin{pmatrix} \cos\theta_2 \cos\theta_3 & \sin\theta_1 \sin\theta_2 \cos\theta_3 + \cos\theta_1 \sin\theta_3 & -\cos\theta_1 \sin\theta_2 \cos\theta_3 + \sin\theta_1 \sin\theta_3 \\ -\cos\theta_2 \sin\theta_3 & -\sin\theta_1 \sin\theta_2 \sin\theta_3 + \cos\theta_1 \cos\theta_3 & \cos\theta_1 \sin\theta_2 \sin\theta_3 + \sin\theta_1 \cos\theta_3 \\ \sin\theta_2 & -\sin\theta_1 \cos\theta_2 & \cos\theta_1 \cos\theta_2 \end{pmatrix}.$$

The matrix R is the product of the three elementary rotation matrices given by

$$R = R^{(3)} R^{(2)} R^{(1)} = \begin{pmatrix} \cos\theta_3 & \sin\theta_3 & 0 \\ -\sin\theta_3 & \cos\theta_3 & 0 \\ 0 & 0 & 1 \end{pmatrix} \begin{pmatrix} \cos\theta_2 & 0 & -\sin\theta_2 \\ 0 & 1 & 0 \\ \sin\theta_2 & 0 & \cos\theta_2 \end{pmatrix} \begin{pmatrix} 1 & 0 & 0 \\ 0 & \cos\theta_1 & \sin\theta_1 \\ 0 & -\sin\theta_1 & \cos\theta_1 \end{pmatrix}.$$

As we can easily access the coordinates of the points in MeshLab, we can finally rewrite Approximation 4.2 for a similar point i of V_{scan} and $V_{picture}$, both expressed in $[\hat{R}^{VS}]$:

$$\begin{pmatrix} x_{i,p} \\ y_{i,p} \\ z_{i,p} \end{pmatrix} \approx R \cdot \begin{pmatrix} x_{i,s} \\ y_{i,s} \\ z_{i,s} \end{pmatrix} + \begin{pmatrix} X \\ Y \\ Z \end{pmatrix} \tag{4.3}$$

where the $(x,y,z)_{i,p}$ and $(x,y,z)_{i,s}$ coordinates stand for the photographed and the scanned violin respectively. Our fitting problem is now well defined and ready to be solved.

4.3.2 Problem solving

Minimisation of the Euclidean distance

As we know how to map a point onto another, we first thought about minimising the average Euclidean distance between known similar points of one cloud and the mapping

of the second. Hence, we initially took the 8 points corresponding to the 8 corners on the two clouds and minimised the averaged sum of their distances with

$$\min \frac{1}{n} \sum_{i=1}^{n=8} \left| \begin{pmatrix} x_{i,p} \\ y_{i,p} \\ z_{i,p} \end{pmatrix} - \left[R \cdot \begin{pmatrix} x_{i,s} \\ y_{i,s} \\ z_{i,s} \end{pmatrix} + \begin{pmatrix} X \\ Y \\ Z \end{pmatrix} \right] \right|$$

in order to find the 6 parameters X, Y, Z, θ_1, θ_2 and θ_3, where $|\cdot|$ is the vector norm operator.

This formulation works with Python minimisation functions (more on this below), but suffers from a major issue. Indeed, we have to manually select the points of interest in MeshLab on the two meshes, and then encode them in Python. Two problems arise from that:

- As the selection is manual, we can only take into account a limited number of points. Otherwise, the encoding would take too long.
- As the meshes are dense, it is really difficult to manually select with sufficient accuracy the precise points that are similar from one cloud to another (here, the 8 corners).

We then thought of automating our process to consider all points directly in Python and not manually in MeshLab. But once again, problems appeared: the clouds do not have the same number of points and are not indexed in the same way. It is therefore impossible to use a single loop with the same index or two loops with different indices. Indeed, the point i of a cloud will not correspond to the point i of the other. And if we consider the point i on one side and the point j on the other, how could we guess the correct indices of i and j to know that these particular points are related ? This would bring us back to our original problem of finding the point on one side that best matches a point on the other side... So we had to abandon this approach of manually finding matching points in both frames and had to think of something else. Thanks to Prof. Jean-François Remacle [15], expert in numerical geometry, we were advised on some tools to compare two dense clouds. We focused on the Fast Library for Approximate Nearest Neighbours (FLANN) which will be described in the next section.

Minimisation of the distance with the Fast Library for Approximate Nearest Neighbours (FLANN)

The FLANN algorithm consists in finding, for each node of a given test point cloud, its k nearest nodes in a given data cloud and the distances that separate it from them (in our case, we only need $k = 1$ neighbour). Thus, two identical point clouds considered as the data and test sets will have a distance of 0 mm for each node, as each node on one cloud will be its own closest neighbour on the other cloud. It should be noted, however, that the algorithm does not take into account the potential transformation of the clouds. This means that if, for example, the test set is the same as the data set but with a rotation of 90°, the algorithm will not return a distance of 0 mm for each node. Thus, we come back exactly to our initial fitting problem, but this time, we have a tool that allows us to consider all the nodes. Indeed, thanks to the *flann* library in [17], we can easily specify a data and a test sets to the FLANN function which will return, for each node of the test set, the index of the closest point of the data set and the distance between them.

15. `https://uclouvain.be/fr/repertoires/jean-francois.remacle`

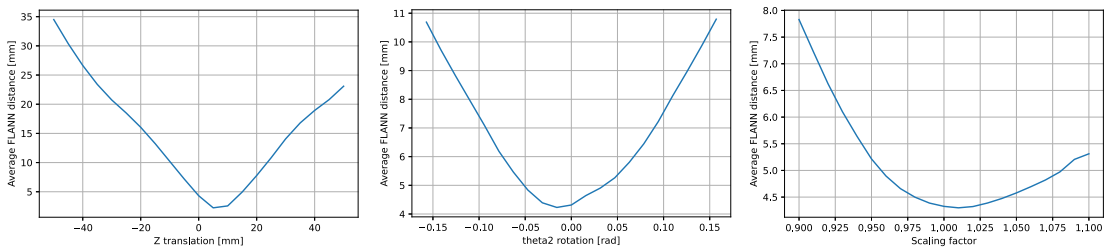
We only need to average these distances to get the total averaged FLANN distance to be minimised (which is identically equivalent to minimising the averaged Euclidean distance as mentioned above, but we preferred to call it differently to dissociate the two different approaches).

In addition, at this stage, we reconsidered the manual scaling performed with the photogrammetric mesh and the swelling effect of the bubble reconstruction for the DICOM mesh. We concluded that it would make sense to include a scaling parameter K in the optimisation problem to better fit the point clouds. Hence, we want now to find the 7 optimal parameters (the six previous ones and K) such that

$$V_{picture} \approx K \left[R \cdot V_{scan} + \begin{pmatrix} X \\ Y \\ Z \end{pmatrix} \right] \qquad (both\ expressed\ in\ [\hat{R}^{VS}]) \tag{4.4}$$

Initialisation

The optimisation process was carried out with a built-in minimisation function in Python. The process is very long. The meshes to be compared being huge, a single call of the FLANN function can take up to 35 *sec* and the whole process about 13 *hours*. We must therefore initialise our algorithm well to limit the computational time. To do so, we evaluated the FLANN distance between the meshes by changing each parameter one by one. As we stated in the beginning of this chapter, the translations were set up manually, so the minimum values are not especially located when the parameter does not change. However, we can observe that for the rotations, the minimum is really close to 0 *rad* for both violins, which proves that the PCA alignment has been effective. Here is an example of this individual evaluation, parameter by parameter, for the Hofmans 2846 (similar graphs are obtained for the Cuypers 2833). The shape of the graphs suggests there will not be local minima troubles in the optimisation process. Indeed, they are monotonically increasing on both sides of the minimum value. The X and Y translations, as well as the θ_1 and θ_2 rotations provide similar plots.



(a) *Z translation*
min in $Z = -7.5$ $[mm]$

(b) θ_2 *rotation*
min in $\theta_2 = \frac{-\pi}{200}$ $[rad] \approx \frac{-3}{10\ 000}$ $[°]$

(c) K *scaling*
min in $K = 1.01$

FIG. 4.16 – *FLANN minimisation for each individual parameter*

We can now initialise our minimisation process with each individual value returned for the two violins.

Optimisation methods

The library *scipy.optimize*[16] provides a large number of built-in minimisation functions. We are interested in the modified Powell algorithm[17]. Indeed, this function does not need to receive the derivatives of the objective function as arguments. As mentioned above, we want to minimise the total average distance between all points from one cloud to the other. To obtain all the distances, we used the built-in FLANN function as a black box, and thus we only have access to the numerical value of the distance but no further information such as derivatives. We then chose the Powell minimisation method. We tried out of curiosity other methods such as the Nelder-Mead algorithm (simplex) or Broyden–Fletcher–Goldfarb–Shanno (BFGS) algorithm. The first one does not need the derivatives of the function either and the second one automatically computes them based on numerical methods. However, these two functions stopped running after a very long time without reaching convergence. Here is the summarised procedure:

- Initialisation of a x_0 vector based on the individual minimisation of the 7 parameters.
- Application of the modified Powell's algorithm which will call a large number of times the objective function to be minimised (including a call of the FLANN function each time) and update its parameters until convergence. Each iteration takes about 35 *sec*.

Results of the minimisation

We can find the results of the fitting problem on Table 4.1. We tried to optimise the average distance between the points with and without the scaling factor K.

Violins	Without K	With K
Hofmans 2846	0.94 mm	0.72 mm
Cuypers 2833	1.02 mm	0.32 mm
Average running time	$\approx$ 470 iterations ($\approx$ 4,5 $hours$)	$\approx$ 1430 iterations ($\approx$ 13 $hours$)

TAB. 4.1 – *Results of the fitting problem*

We can draw several conclusions from this table. First, the average error lies in the mm range, which is small. The fitting is not perfect, but taking into account the insertion of several errors during the construction process (averaging of distances in MeshLab for the scaling, small holes on the DICOM mesh, ...), we can still be satisfied. Then, we can see that it was indeed a good idea to add the scaling factor K. Both results are better

16. `https://docs.scipy.org/doc/scipy/reference/optimize.html`

17. `https://docs.scipy.org/doc/scipy/reference/generated/scipy.optimize.fmin_powell.html`. Here is the description we can find in the Python documentation: *Uses a modification of Powell's method to find the minimum of a function of N variables. Powell's method is a conjugate direction method.*

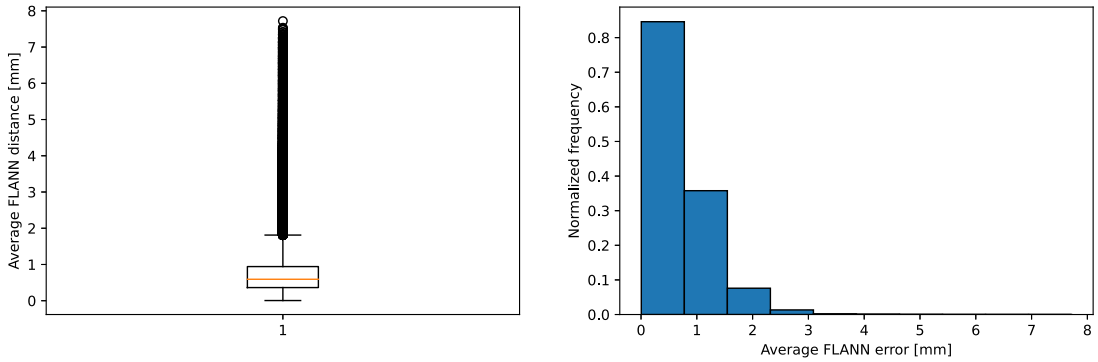
The algorithm has two loops. The outer loop merely iterates over the inner loop. The inner loop minimizes over each current direction in the direction set. At the end of the inner loop, if certain conditions are met, the direction that gave the largest decrease is dropped and replaced with the difference between the current estimated x and the estimated x from the beginning of the inner-loop.

The technical conditions for replacing the direction of greatest increase amount to checking that

- *No further gain can be made along the direction of greatest increase from that iteration.*
- *The direction of greatest increase accounted for a large sufficient fraction of the decrease in the function value from that iteration of the inner loop*

when we consider it in the minimisation problem, especially for the Cuypers 2833 whose average distance is reduced by a factor 3. It it therefore a really nice gain. However, the convergence is much slower because of this new variable to be optimised in the problem.

We finally asked ourselves if computing an average distance was not too unrepresentative of the trends of the whole point clouds. We therefore decided to display a box plot and a histogram of the distances distribution. The density of the histogram is normalised, such that the integrated area under the bins sums up to 1. These results hold for the Hofmans 2846 with the factor K but once again, similar ones are obtained for the Cuypers 2833.



(a) *Box plot of all the distances*

(b) *Distribution of the distances*

FIG. 4.17 – *Distances distribution representations (with K)*

We observe directly that there are many outliers whose distance to the nearest neighbour is much higher than the average (the maximum goes up to 8 mm). We decided to filter this distribution in two ways. On the one hand, by eliminating the points whose distance to the nearest neighbour is greater than the mean distance μ, plus the standard deviation σ of the set. On the other hand, by removing those whose this distance is greater than $Q_3 + 1.5IQR$, Q_3 being the third quartile of the distribution and IQR the interquartile range[18]. We have only filtered the distances on one side, as small distances are relevant and sign of optimality. Filtered results are shown in Table 4.2.

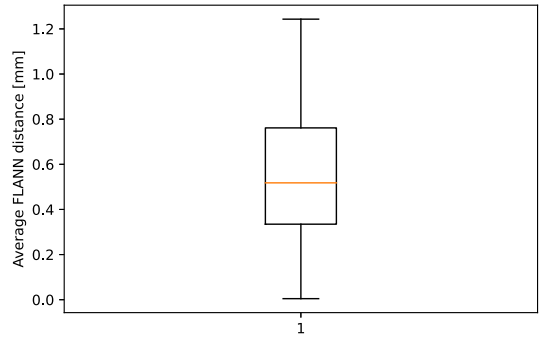
Filtering	μ'	σ'	μ"	σ"
None	0.72 mm	0.52 mm	0.32 mm	0.25 mm
$dist < \mu + \sigma$	0.56 mm	0.28 mm	0.29 mm	0.10 mm
$dist < Q_3 + 1.5IQR$	0.66 mm	0.39 mm	0.29 mm	0.11 mm

TAB. 4.2 – *Means and standard deviations after filtering for Hofmans 2846 (prime, left) and Cuypers 2833 (second, right)*

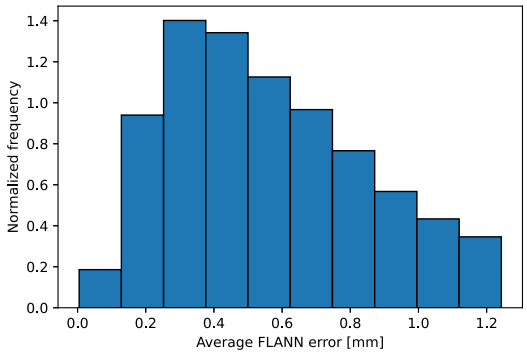
Hence, by filtering, we further improved the fitting result. For the Cuypers 2833, as the average distance was already small, the filtering mainly reduced the standard deviation

18. A statistical set can be divided into quartiles, i.e. in four parts containing the same amount of data. The 3 values that determine the intervals (excluding the minimum and maximum values of the distribution, which are the outer values) are called the three quartiles: Q_1, Q_2 and Q_3. The interquartile range is equal to $IQR = Q_3 - Q_1$. Outliers are often defined as data that do not belong to the interval $[Q_1 - 1.5IQR\ ,\ Q_3 + 1.5IQR]$.

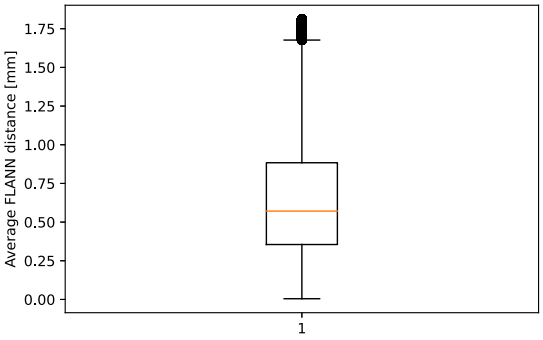
than really improving the mean. The new distributions and box plots are presented in Figure 4.18 for the Hofmans 2846, still with the parameter K.



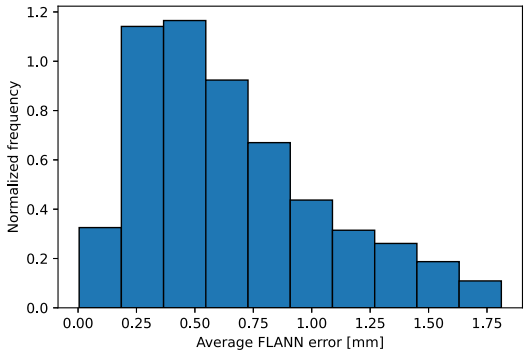
(a) *Box plot of the distances lower than* $\mu + \sigma$



(b) *Distribution of the distances lower than* $\mu + \sigma$



(c) *Box plot of the distances lower than* $Q3 + 1.5IQR$



(d) *Distribution of the distances lower than* $Q3 + 1.5IQR$

FIG. 4.18 – *Filtered distributions*

As the whole set of distances is plotted on histograms, we conclude that the filtering eliminates all the outliers which resulted in a distance greater than 1.25 mm or 1.80 mm, which is significantly better than the original set with distances up to almost 8 mm. These are also excellent statistics on our results.

We can conclude that this optimisation problem yielded good results. As we mentioned, we have induced errors during the process, but we can still obtain a small average distance which can be improved by filtering. However, under an average distance of a few tenth of mm, we can conclude that a match is possible and that we do not even need to use a filter. Indeed, because of all the induced errors we have already mentioned, it will be very difficult, and probably even impossible, to fit the two point clouds perfectly. But the sufficiently small value we obtained proves that we can continue our research without doubting the reliability of the photogrammetric violin.

Hence, we could summarise this chapter as follows. First, we processed the photogrammetric mesh by scaling it and orienting it along the axes of the reference frame we defined and showed in Figure 4.3. Then, we reconstructed a mesh from the DICOM files in order to compare similar 3D objects. Finally, we explained how to check the correspondence between the point clouds and concluded that the photogrammetric mesh is precise enough to

continue our analysis. The optimised average distance can be improved by filtering, but as we said, we just wanted to check whether our point cloud (and thus our mesh) was precise enough. Results in Table 4.1 proved that it was indeed. In the following chapter, we will abandon the DICOM mesh and focus only on the photogrammetric one in order to find the violins characteristic points and to validate our objectives.

Chapter 5

Characteristic points study

Now we are sure that our two photogrammetric meshes are ready to be used, we will show how to process them to compute features such as minima and inflection points. Some of the algorithms and methods described in this chapter come from R. Lothaire's thesis [11]. They have been adapted to our needs, especially as we handle meshes and R. Lothaire did not: he was using black and white matrices of pixels instead. However, the main ideas were already thought of. First, we will see how to make good planar sections and then how to find the characteristic points from them.

5.1 Cutting through the mesh

We use the Python library *meshcut* [16] to perform plane cuts through the mesh. But before we can do this, we still need to export our data from MeshLab to Python and lay the groundwork for accurate slicing. The cutting process will be explained in this section as follows.

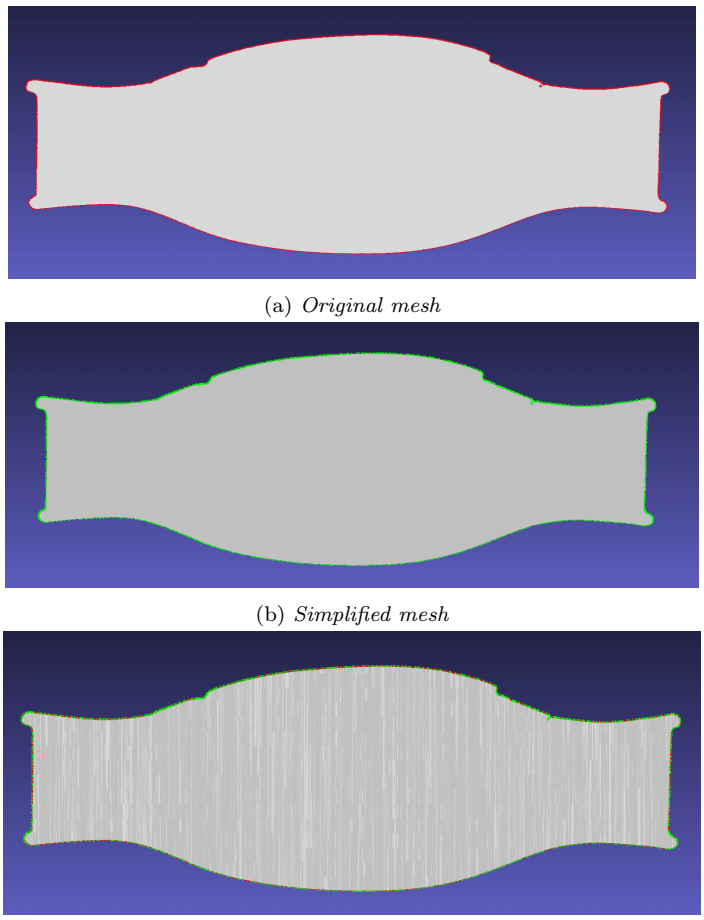
- Mesh simplification
- Sound board and back separation
- Violin edges delimitation
- Planar sections through the mesh
- Sound board or back identification in the cross section

The first two steps are still performed in MeshLab and the last three in Python.

5.1.1 Mesh simplification

As the meshes received by I. Thys are composed of 1.5 million points for 3 million faces, the cutting process will be very long if we do not simplify them. MeshLab has a mesh reduction system that preserves the delimitations and orientation of the faces. We can encode in this built-in function the number of faces or vertices we want to reach. We have arbitrarily chosen to keep 500 000 faces. In order to ensure that we did not lose too much information, we performed cross sections in the original and simplified meshes using the built-in cut tool in MeshLab. This function returns a set of polylines (points connected by line segments) delimiting the perimeter of the cut. We can also reconstruct a surface between these polylines to better visualise the cut. Thus, we see in Figure 5.1 the cross section of the original Hofmans 2846 mesh (red) and the simplified one (green). They overlap almost perfectly. The simplified mesh has fewer points than the original one (about twice less), but those points are still well located on the perimeter and we therefore

do not lose any information about the cuts shape. We can see on the cross sections the small depressions due to the F-holes, as explained in Chapter 3.



(a) *Original mesh*

(b) *Simplified mesh*

(c) *Both overlapping*

FIG. 5.1 – *Cross sections in MeshLab*

This simplification step may seem contrary to I. Thys' work, but it is not the case. Indeed, working with a 'small' mesh from the beginning does not guarantee that it will be accurate. However, here, as we have pushed the level of precision far, we know that the simplification tools will take this original accuracy into account. Thus, the simplified mesh will be still as qualitative because it remains sufficiently close to the original one, even with fewer faces and nodes. We will therefore continue with a mesh of 500 000 faces.

5.1.2 Sound board and back separation

We want to make a separate analysis of the sound board and the back. We therefore do not need a mesh that includes the whole body of the violin anymore. On the one hand, this will make the resulting mesh even lighter than 500 000 faces, and on the other hand, the analysis of these precise areas will not be disturbed by extraneous elements. MeshLab allows us to do this quickly. We therefore remove from our mesh all the points that do not concern the back or the sound board. Each isolation is done individually so that we can concentrate on one sub-mesh at a time. They can be seen put back together in Figure 5.2. We have removed the fingerboard area from the two violins to make a similar approach for both. Indeed, although we showed in Figure 4.2 that we could recreate surfaces to fill

holes in the Cuypers 2833 sound board, the process would have created mesh irregularities that our program may misinterpret. We therefore preferred to remove the fingerboard for the sound board analysis.

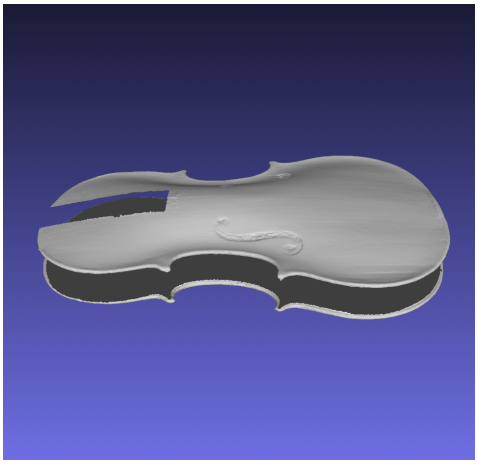


FIG. 5.2 – *Isolated sound board and back*

In his thesis, R. Lothaire did not separate the sound board and the back beforehand and therefore worked with a single violin from which he isolated both parts numerically. In addition, he analysed both of them viewed from above and hence proposed an analysis of the back from the inside of the soundboard. To illustrate our point, the soundboard was mapped as a mountain and the background as a valley. However, it is preferable to analyse the back and the sound board in the same way, which is more logical from an organological point of view. It also allows the same code to be used on both sides and not to recreate a symmetrical one for the back analysis. So, using MeshLab's rotation tool, we turned the back around to adopt a similar orientation to the sound board. We can see the two elements placed side by side in Figure 5.3. Our sub-meshes are now completely ready to be exported into Python. As the reasoning is now the same for the sound board and the back, we will use the general term sound board for both.

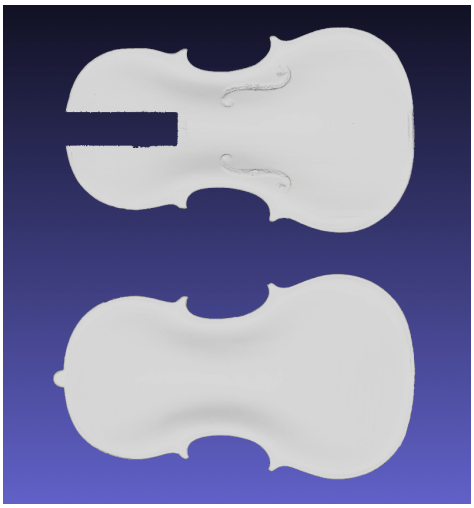


FIG. 5.3 – *Top view of sound board and back*

5.1.3 Violin edges delimitation

The Python library *plyfile* [15] allows to read and write .ply files. It is therefore easy to transfer our data from MeshLab to Python. As mentioned earlier, we want to make our planar cuts based on a top view of the sound board. Figure 5.4 shows in general terms what we have done in Python to process our data and define precisely the planar sections on which we can find our points of interest. Each algorithm or function will be detailed below.

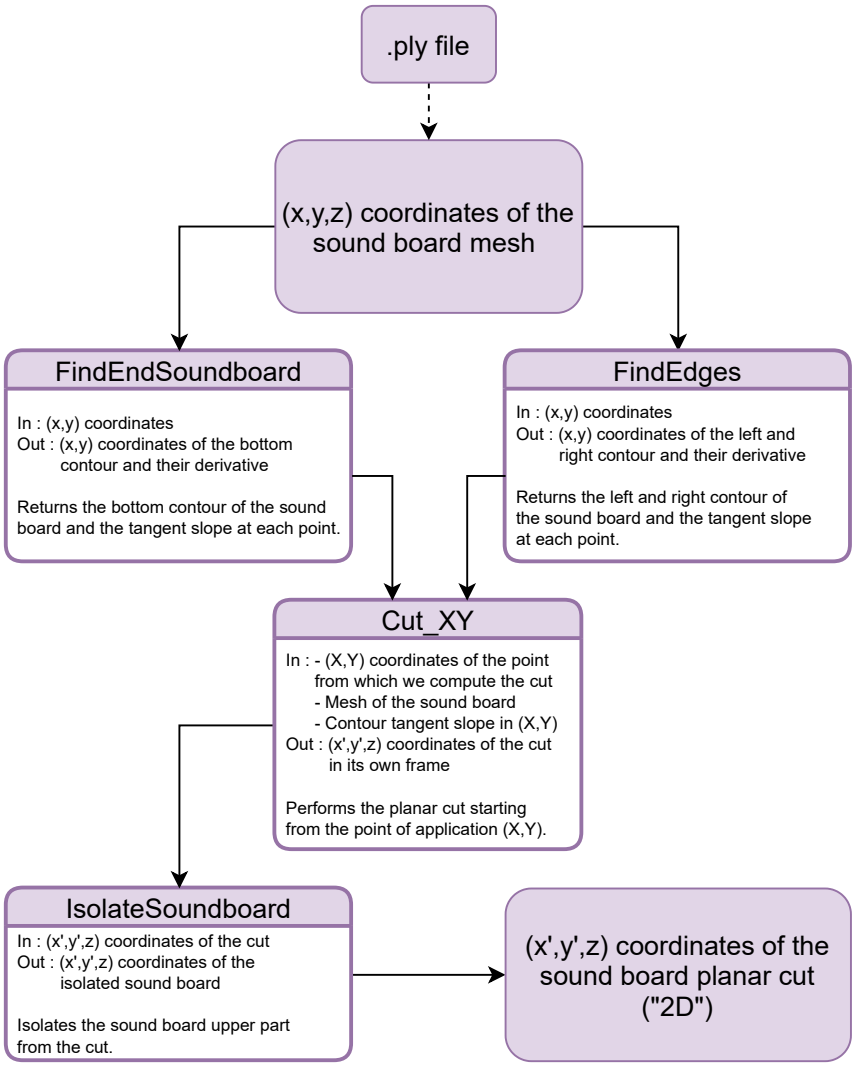


FIG. 5.4 – *General Python process of the sound board coordinates isolation*

From the violin top view, we need to keep only the points that delimit its contour. Thanks to the organological properties of the violin, we know that the extreme points on the y-axis belong to the sound board. All we need to do is to design a program that will go through the x-axis and keep the maximum and miminum ordinates that will correspond to the sound board contour. As we have seen in the previous chapter that the PCA alignment was optimal, we can use a 2D approach without losing information. We therefore do not need the z-coordinates, the top view of the (x,y) will be sufficient. We have chosen to discretise our x-axis every mm. We will loop through this discretised x-axis and evaluate

all the ordinates in a bandwidth of 1 mm centred on each $x_{discrete}$. The contour points will therefore be the maximum and minimum of each bandwidth. Once the sound board is defined in a discrete way, we will approximate its raw contour using cubic splines[19]. Algorithm 1 shows how to do this.

Algorithm 1 FindEdges Function

Input:

x, $y \in \mathbb{R}^{m\times 1}$, abscissae and ordinates of the point cloud

Output:

x_{up}, $x_{down} \in \mathbb{R}^{n\times 1}$, abscissae of the right and left parts of the sound board[20]
y_{up}, $y_{down} \in \mathbb{R}^{n\times 1}$, ordinates of the right and left parts of the sound board
spl_{up}, $spl_{down} \in \mathbb{R}^{n\times 1}$, spline approximation of the ordinates
tan_{up}, $tan_{down} \in \mathbb{R}^{n\times 1}$, derivatives of the spline approximation

Algorithm:

Initialise $x_{discrete}$ ▷ x_{up} or x_{down}
for $i = 1, \ldots, n$ **do** ▷ Raw contour
  mask = ordinates of the $x \in [x_{discrete,i} - 0.5 \ ; \ x_{discrete,i} + 0.5]$ ▷ 1 mm bandwidth
  $y_{up,i} = max(mask)$
  $y_{down,i} = min(mask)$

Compute the spline approximation of the contours $\Longrightarrow$ spl_{up}, spl_{down} ▷ Spline contour
Compute the derivative of the splines $\Longrightarrow$ tan_{up}, tan_{down}

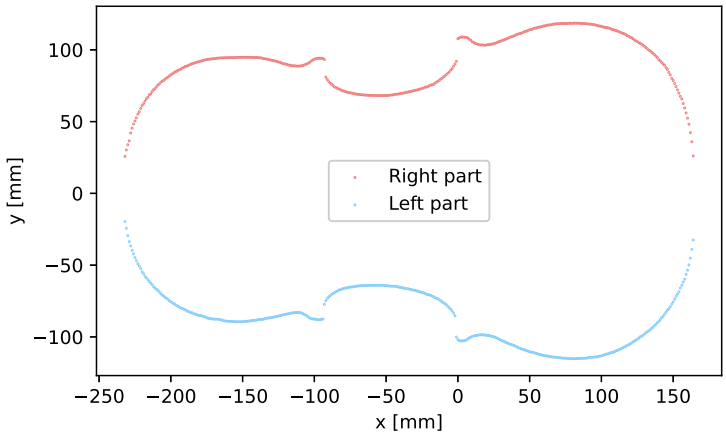


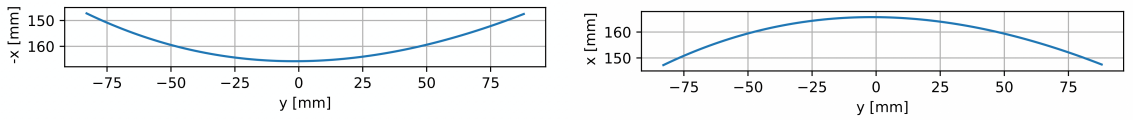
FIG. 5.5 – *Discrete contour of the Hofmans 2846 soundboard*

Figure 5.5 shows that the discretisation of the x-axis every mm seems precise enough

19. The adjustment will be made by minimising the difference between the raw data and their approximation. An interesting comparison can be found in [19].

20. These two variables are the discretisation of the x axis at each mm, $x_{discrete}$. As the violin is symmetrical, they are in fact equal but we have separated them for the sake of clarity.

to reconstruct most of the left and right parts of the sound board. However, since the layout of the very end is almost as straight as a vertical line, it is not sufficient searching for the last points in a bandwidth of 1 mm. We should proceed with a much smaller width for the end, but it is a bit tedious to have one vector with different scales. So we decided to approach the problem from the other direction. Indeed, we placed ourselves in a $y - x$ frame instead of our usual $x - y$ to study the curvature of the soundboard bottom. We had to face orientation issues but these were quickly solved. First, we had to recode the *FindEdges* function to fit the $y - x$ frame. We can see this new formulation in Algorithm 2. Then, our approach suggests that we are looking for a minimum, but from our initial x axis, we are actually looking for the maximum x to define the end of sound board, as we can see in Figure 5.7. We finally note that we have increased the bandwidth to 2 mm. With only 1 mm, some points had no maximum and our algorithm returned strange results.



(a) *Intuitive curvature on reversed x axis*

(b) *Mathematical representation on x axis*

FIG. 5.6 – *Intuitive and mathematical representations of the sound board bottom*

Algorithm 2 FindEndSoundboard Function

Input:

x, $y \in \mathbb{R}^{m\times 1}$, x- and y-coordinates of the cloud

Output:

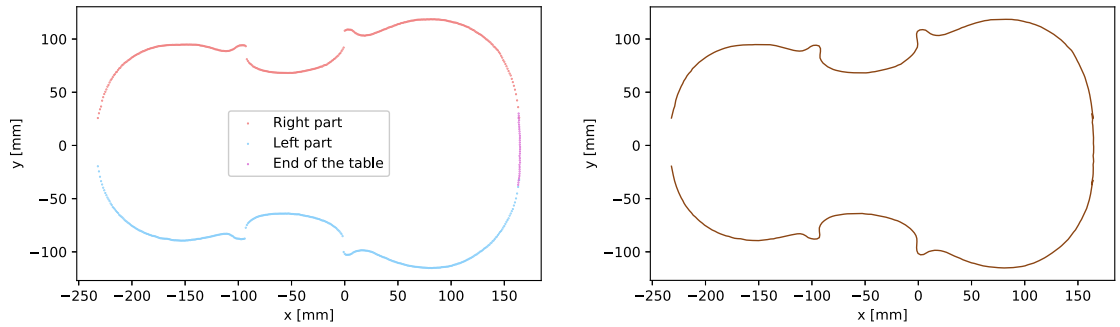
x_{right}, $y_{right} \in \mathbb{R}^{p\times 1}$, coordinates of the sound board bottom
$spl_{right} \in \mathbb{R}^{p\times 1}$, spline approximation of the bottom
$tan_{right} \in \mathbb{R}^{p\times 1}$, derivatives of the spline approximation

Algorithm:

Keep only the points on the last 1 mm of the x-axis
Initialise y_{right}, discretisation of the y axis every mm for these kept values
for $i = 1, \ldots, p$ **do** ▷ We are working on a y-x frame and not a x-y anymore
mask = x-coordinates of the $y \in [y_{right,i} - 1 \ ; \ y_{right,i} + 1]$ ▷ 2 mm bandwidth
$x_{right,i} = max(mask)$

Compute the spline approximation of the bottom $\Longrightarrow spl_{right}$ ▷ Spline contour
Compute the derivative of the spline $\Longrightarrow tan_{right}$

The results of this new approach, combined with the one for the side parts, provided a nice approximation of the sound board as shown in Figure 5.7a. We then displayed in Figure 5.7b the approximation of the contour with cubic splines. We fitted the points into a single curve for a better visualisation. However, to keep the accuracy of what we calculated before, we will continue with the derivatives computed on the three splines approximation for the three parts (left, right, bottom), and not directly the derivatives of this unique curve. In the next figures, the brown curve will be considered as the contour of the sound board and will not be captioned anymore.

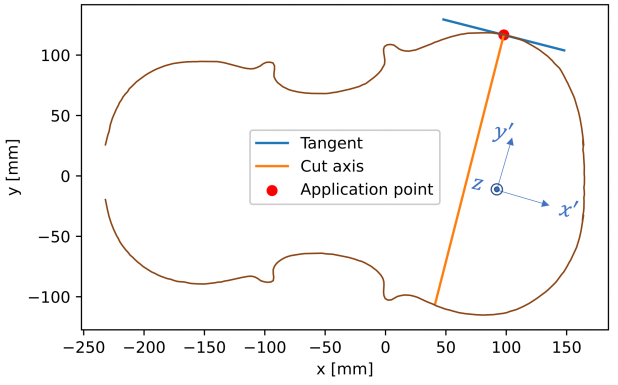


(a) *Discrete* (b) *Spline*

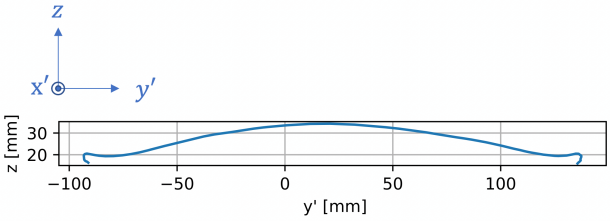
FIG. 5.7 – *Discrete and spline approximation of the Hofmans 2846 sound board*

5.1.4 Planar sections through the mesh

We have now a nice outline of the sound board and we know the tangent slopes at each point of it. Given the vertices and faces of the mesh, the application point and the normal to the cut (i.e. the tangent slope), the *meshcut* function [16] returns a planar cut normal to the tangent at the application point, as a set of polylines. This function is powerful because the cuts are done through the mesh and not the point cloud. We can therefore keep the precision of the faces and not approximate a cut from the point cloud, which is not negligible in our research. Algorithm 3 shows how we proceed to obtain a cut from a 2D top view. It is important to note that once we have made a cut, we will work in its own frame (x',y',z) to compute the characteristic points. We will convert them to the original frame (x,y,z) at the end of the computations. Figure 5.8 shows a planar cut and the frame in which it is defined.



(a) *Top view in* (x,y,z)



(b) *Cross section in* (x',y',z)

FIG. 5.8 – *Planar cut in both frames*

Algorithm 3 Cut_XY Function

Input:

x_{absc}, $tan_{absc} \in \mathbb{R}^{n\times 1}$, abscissae of the points on which we will proceed the cut and their derivatives $\Longrightarrow$ either x_{up} and tan_{up}, x_{down} and tan_{down} or y_{right} and tan_{right} [21]

X, $Y \in \mathbb{R}$, coordinates of the point from which we will cut the mesh

$verts$, $faces$, vertices and faces of the sound board mesh

Output:

$cut \in \mathbb{R}^{3\times q}$, ($x$,$y$,$z$) coordinates of the polylines of the cut

$cut_rot \in \mathbb{R}^{3\times q}$, ($x'$,$y'$,$z$) coordinates of cut

$ax \in \mathbb{R}$, x'-axis of cut

$a \in \mathbb{R}$, slope of the tangent in (X,Y)

Algorithm:

Compute the tangent slope in (X,Y) $\Longrightarrow a$ ▷ Given tan_{absc}

Compute cut with the *meshcut* function ▷ Given X, Y, $verts$, $faces$ and a

Compute cut_rot, the coordinates of cut in the frame (x',y',z)

5.1.5 Sound board or back identification

The cut shown in Figure 5.8b still contains rounded overhanging edges on the left and right sides. We want to eliminate them to isolate the upper part of the sound board (i.e. without the overhanging edges). We applied a technique similar to Algorithms 1 and 2, described in Algorithm 4. It might be possible that some points of the sound board are not defined because of an interruption in the polylines of the cut. These points will thus be approximated by the average of their two neighbours [22]. The interest of averaging is shown in Figure 5.9. The large depression in the middle of the cut is due to the removal of the fingerboard.

21. x_{absc}, $tan_{absc} \in \mathbb{R}^{p\times 1}$ in that third case

22. This reasoning is based on a strong assumption that any point, out of the fingerboard area, that is not defined is surrounded by two defined neighbours. The hypothesis has been verified throughout our planar cuts.

Algorithm 4 IsolateSoundboard Function

Input:

$cut_rot \in \mathbb{R}^{3\times q}$, coordinates of the planar cut in (x',y',z)

Output:

$soundboard_abs$, $soundboard_ord \in \mathbb{R}^{k\times 1}$, the (y',z) coordinates of the sound board upper part

Algorithm:

Initialise $soundboard_{abs}$, discretisation of the y' axis every mm

for $i = 1,\ldots,k$ **do**

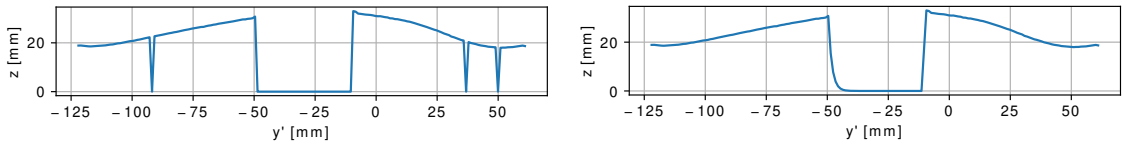
mask = z-coordinates of the $y' \in [soundboard_abs_i - 0.5\ ;\ soundboard_abs_i + 0.5]$

$soundboard_ord_i = max(mask)$

for $i = 2,\ldots,k-1$ **do** ▷ Extremities are defined

if $soundboard_ord_i$ is non defined **then**

$soundboard_ord_i = \frac{soundboard_ord_{i-1}+soundboard_ord_{i+1}}{2}$ ▷ Averaging



(a) *Before averaging* (b) *After averaging*

FIG. 5.9 – *Effect of the averaging on the non defined points*

Now that we have a cut of the isolated upper part of the sound board, as in Figure 5.10, we will see in the next sections how to compute the characteristic points on it.

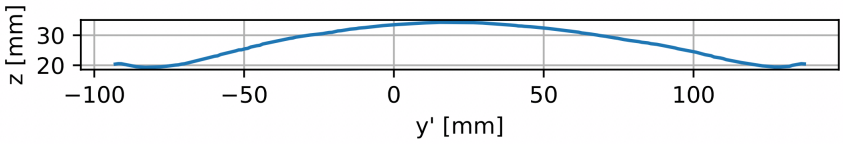


FIG. 5.10 – *Upper part of the sound board without overhanging edges*

5.2 Location of the minima channel

The cut in Figure 5.10 is still a set of polylines. This means that we can easily access the (x',y',z) coordinates of the points. Therefore, we only have to select the one with the lowest ordinate on our research side, which will be our minimum, and express its coordinates in the reference frame (x,y,z). Figure 5.11 shows the procedure we followed to determine the minima on each cut.

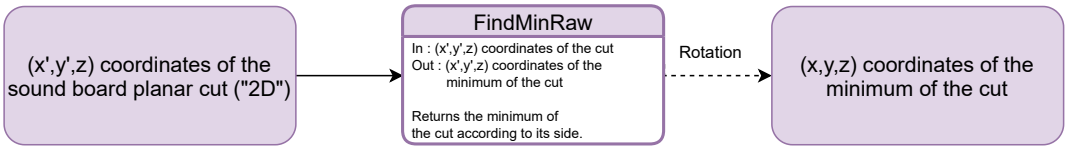


FIG. 5.11 – *Computing minima process*

As we have an a priori knowledge of the minima location, we define a search zone on each planar section. Depending on the side from which we have created the cut, we limit the search zone to one eighth of the sound board, either to the left or to the right. Algorithm 5 shows how to proceed.

Algorithm 5 FindMinRaw Function

Input:

$soundboard_abs$, $soundboard_ord \in \mathbb{R}^{k\times 1}$, the (y',z) coordinates of the sound board upper part

$ax \in \mathbb{R}$, x'-axis of cut

$position$, a string = $right$ or $left$ stating the side on which we look at

Output:

min_coords, the minimum coordinates in (x',y',z)

Algorithm:

$search_zone = \frac{1}{8} soundboard_abs$ in the $position$ side of the soundboard

Find the minimum in $search_zone \Longrightarrow min_coords$

The coordinates obtained are still in (x',y',z). The conversion from one frame to the other is simple. Indeed, as we know the slope of the tangent a, we only need to rotate the points of $arctan(a)$ to convert the coordinates back to the original frame (x,y,z). We then loop our process around the whole sound board to finally get the channel of the minima. This can be seen in Figure 5.12. The whole computation takes about 1,5.

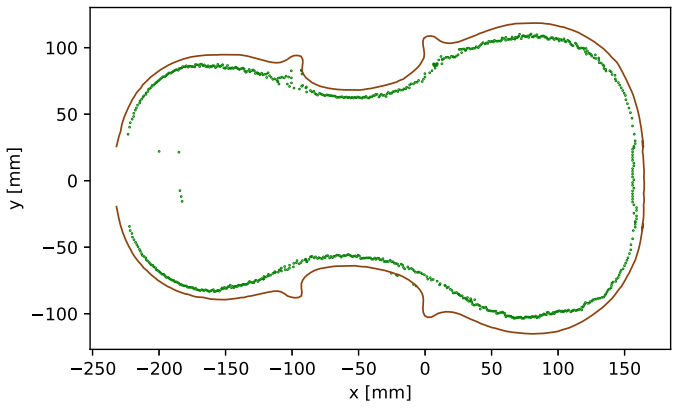
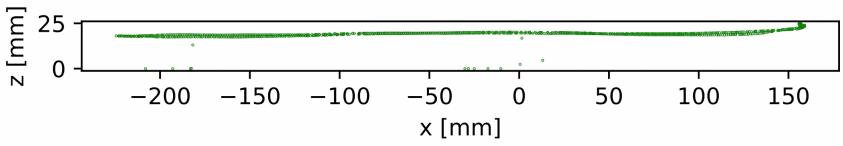
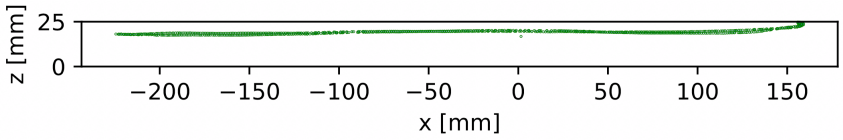


FIG. 5.12 – *Channel on Hofmans 2846 sound board*

Despite a few outliers (notably near the removed fingerboard, the corners and the C-bouts), we see that the x and y coordinates of the minima seem consistent. However, we have no clue about the consistency of the z coordinates. We therefore decided to plot the minima in the xz frame as shown in Figure 5.13a. As there are some outliers, we decided to filter the height distribution in order to eliminate the points whose height is lower than $\mu_z - \sigma_z$, where μ_z and σ_z are the mean and the standard deviation of the distribution. As in our minimisation problem in the last chapter, we decided to perform only one-sided filtering because the problematic outliers are only located at the bottom. We still tried two-sided filtering, but the minima that are slightly higher than the others, but still greater than $\mu_z + \sigma_z$, were eliminated, which reduced the channel information. We can see the plot of the filtered distribution in Figure 5.13b.



(a) *Before filtering*



(b) *After filtering*

FIG. 5.13 – *Profile view of the channel before and after filtering*

These graphs point to a phenomenon that we had not thought to observe but which could still help us to determine whether a violin has been recut or not. Indeed, we see that the minima at the end of the sound board tend to raise up. This characteristic is not observable on a non recut violin, as we can see for the filtered Cuypers 2833 sound board channel in Figure 5.14.

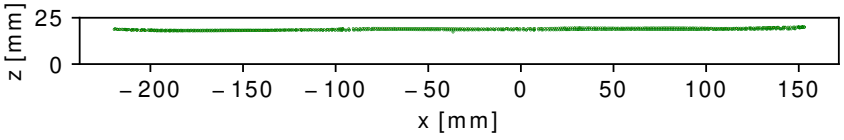


FIG. 5.14 – *Profile view of the filtered Cuypers 2833 sound board channel*

That being said, we can notice in Figure 5.15 that the z outliers of the Hofmans 2846 sound board were also (x,y) outliers. Indeed, from all those we obtained in Figure 5.12 around the fingerboard, the corners and the C-bouts, only three of them remained close to the right corners, one of which is still observable in Figure 5.13b. These three ones are not problematic because we will approximate the channel thanks to splines (the same way as we did with the brown contour) and they will not influence the global fitting on a bad way.

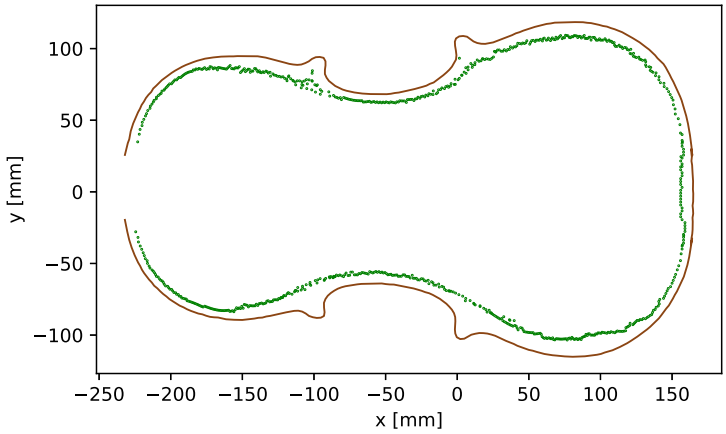
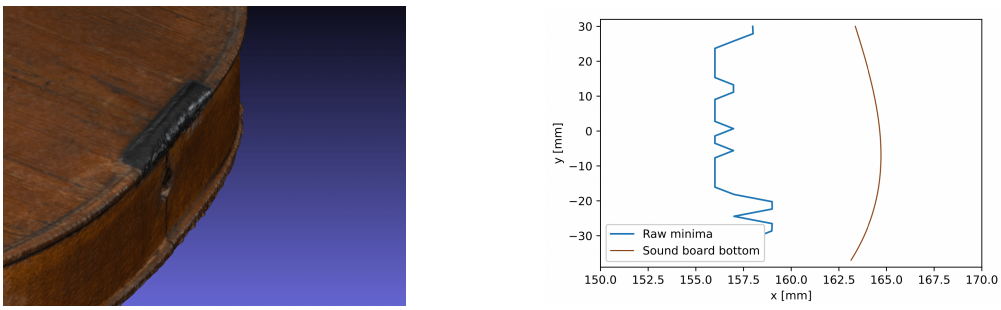


FIG. 5.15 – *Filtered channel on Hofmans 2846 sound board*

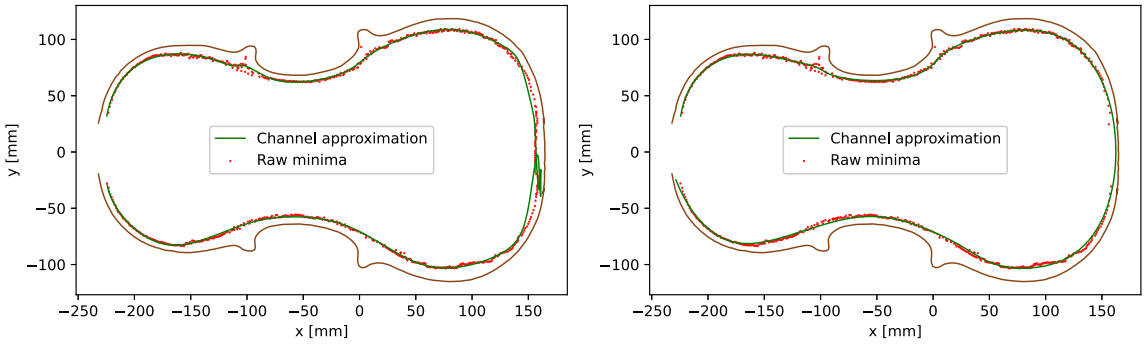
However, the minima near the bottom may be problematic in the spline approximation. Indeed, there is a black border of a few *mm*, called saddle, which influences the location of the raw channel of the recut instrument, as in Figure 5.16a. We can see a zoom on the wrong location of the lower minima in Figure 5.16b. The path is not regular and so this strange arrangement will imply a poor spline approximation of the channel in this area. We can see this bad channel approximation in green and the raw minima in red in Figure 5.17a. The green curve behaves strangely on the edge. However, by removing these lower minima and computing the spline based only on the left and right ones, we can greatly improve the channel approximation. Figure 5.17 shows the difference between the two methods.



(a) *Saddle*

(b) *Disposition of the raw minima*

FIG. 5.16 – *Impact of the saddle on the minima location*



(a) *With the bottom raw minima*

(b) *Without the bottom raw minima*

FIG. 5.17 – *Channel approximation with or without considering the bottom raw minima*

Even though the spline approximation has a better plot, it is still interesting to refer to the raw data to assess its quality.

5.3 Location of the inflection points path

The inflection points computation is similar to that of the minima. However, as we saw earlier with the channel, the cuts may differ from each other depending on whether or not they include the area of the removed fingerboard. Thus, the calculation algorithm had to be rethought.

To avoid focusing on irrelevant points, we define once again a search zone on the isolated sound board. If the cut contains a depression (referred as a hole in the algorithm), we look either to the right or to the left of it depending on the search side. If the cut does not contain hole, then we look at the right or left side of the sound board, up to its maximum. Once the search zone is defined, we approximate its points with a spline[23]. After that, we retain the potential candidates whose second derivative cancels. There may be several depending on how the spline interpolates the search area. We consider that the most likely point in those retained is the one with the largest absolute tangent slope. Indeed, depending on the search side, we look at either the most positive or the most negative tangent. Algorithm 6 takes up these ideas in pseudo-code form. We finally note that the approximated spline may not contain any inflection point. Should it be the case, the algorithm would return 0 and we would not consider that result. We can see in Figure 5.18 the results for a cut that contains a hole and one that does not. Finally, we see what the algorithm returns when it does not detect any inflection point.

23. Although the searching idea is similar, the spline approximation of the upper part of the sound board is the fundamental difference between the calculation of inflection points and minima. Indeed, since notions of derivatives are involved, it is no longer possible to search for the points in a raw way, and it is inevitably necessary to pass by a spline approximation.

Algorithm 6 FindInflectionPoints Function

Input:

soundboard_abs, *soundboard_ord* $\in \mathbb{R}^{k\times 1}$, the ($y'$,$z$) coordinates of the sound board upper part

$ax \in \mathbb{R}$, x'-axis of *cut*

position, a string = *right* or *left* stating the side on which we look at

Output:

pI_coords, the inflection point coordinates in (x',y',z)

Algorithm:

hole = *True* if there is a depression on the cut, *False* otherwise

if *hole* is *True* **then**

search_zone = part of the sound board to the *position* side of the hole

Approximate *search_zone* ordinates with a spline

Find the points whose second derivative is 0

Find the one with the highest absolute value tangent $\Longrightarrow$ *pI_coords*

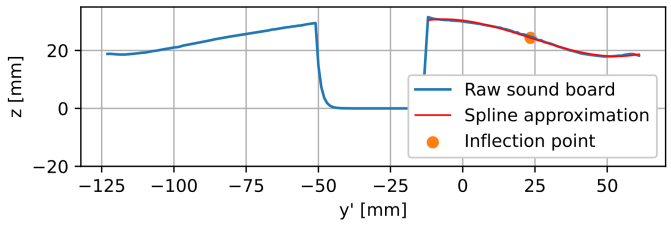
else ▷ There is no hole

search_zone = *position* side, until the maximum of the cut

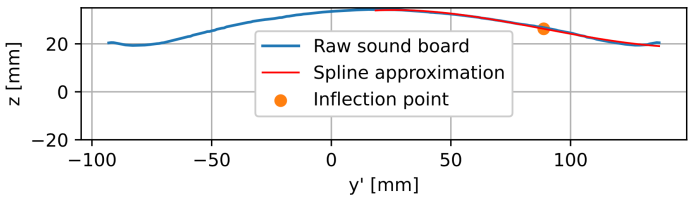
Approximate *search_zone* ordinates with a spline

Find the points where the second derivative is 0

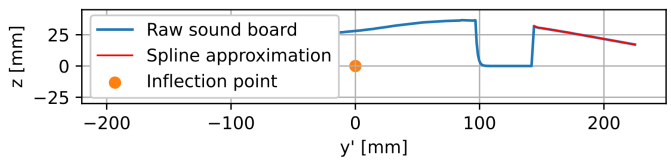
Find the one with the highest absolute value tangent $\Longrightarrow$ *pI_coords*



(a) *Inflection point with hole*



(b) *Inflection point without hole*



(c) *Inflection point not found*

FIG. 5.18 – *Different outputs of Algorithm 6*

By looping the process all along the sound board, we are able to locate the inflection points also in about 1,5 *hour*. Their position is unfortunately a little more scattered than that of the minima and their path approximation is therefore a little less accurate. However, thanks to the same filtering technique as for the minima (removal of the height outliers), we are able to obtain a quite satisfactory result, as we can see for the Cuypers 2833 back in Figure 5.19. It should be noted that almost no inflection points were detected for the bottom of the instruments and that the spline approximation must have predicted them. Thus, this part is rather interpolated than data based.

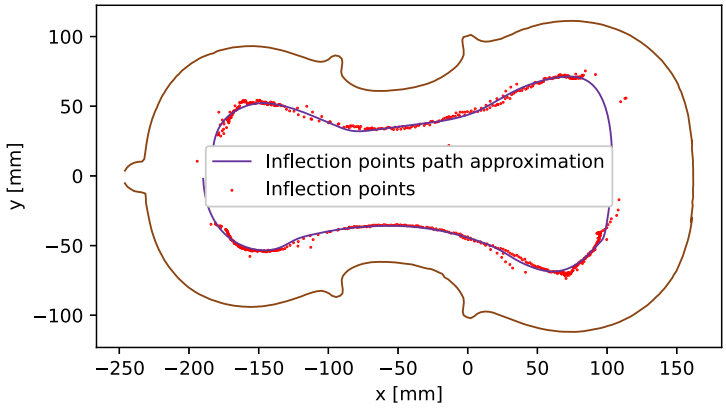


FIG. 5.19 – *Inflection points location*

5.4 Contour lines study

As stated in Chapter 1, the last feature we want to observe on the sound board is the contour lines shape. Their sharpness, in addition to the channel and the inflection path, could help determine whether or not the violin has been reshaped. This contour lines approach appears for the first time in this thesis. In the two previous works [10] [11], the maxima area was evaluated in the same way as the channel and the inflection points. However, the results were not really accurate and therefore it was not possible to conclude anything about this feature. In addition, it is more relevant for drawing conclusions to look at the shape of several contour lines rather than just one for the maxima.

We will use a Python built-in function to return the contour lines of our point cloud. Once again, we justify this approach thanks to the PCA alignment. Indeed, we know that the sound board will be correctly aligned horizontally and that the contour lines will be relevant. The latter are performed every 2 *mm*. We can observe the results for the Hofmans 2846 sound board in Figure 5.20. We can see that the contour lines are estimated at the level of the removed fingerboard, but they are not continuous. We simply ignore this part of the graph in our analysis. Fortunately, the sharpness of the contour lines is similar at the top and bottom of the sound box. Therefore, even if we removed the fingerboard, we still have the information when looking at the bottom. For the back, this will not be a problem as it is still entire and nothing was removed from it.

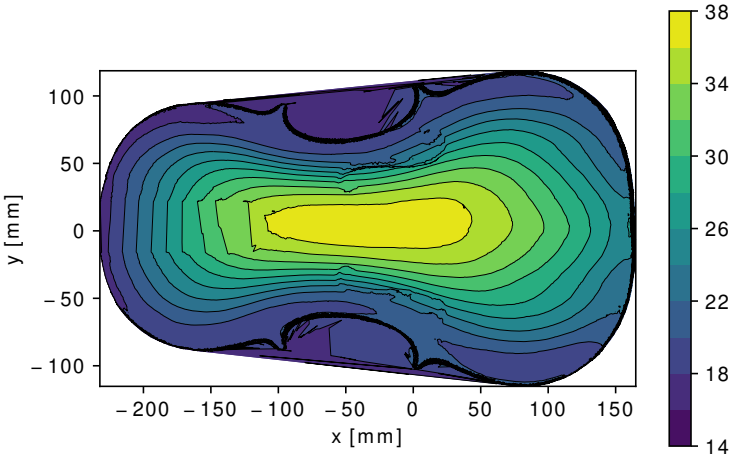
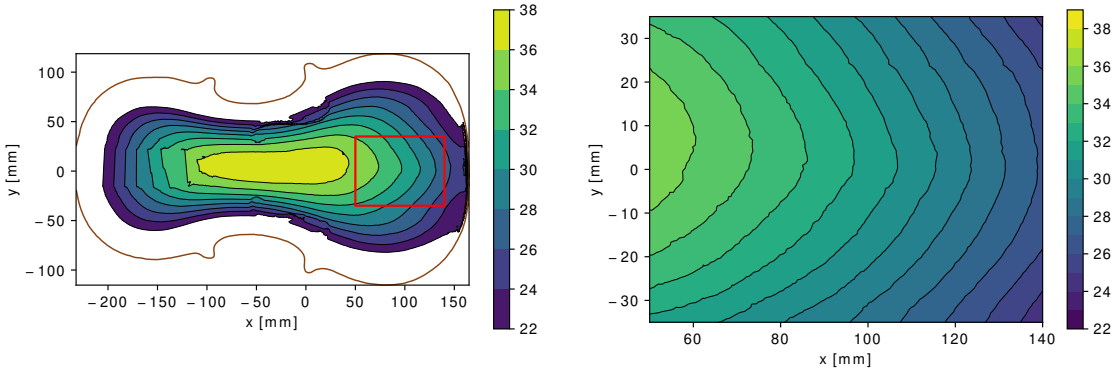


FIG. 5.20 – *Contour lines*

We see in Figure 5.20 that the built-in function also estimates the contour lines outside the sound board, which is neither necessary nor relevant for our analysis. We thus decided to start the contour lines not at the borders but a little further inside the boundary of the sound board. We then zoomed on the bottom and refined the lines every *mm* to observe their sharpness more precisely. This can be seen in Figure 5.21, still for the Hofmans 2846 sound board.



(a) *Relevant contour lines* (b) *Zoom and refinement*

FIG. 5.21 – *Relevant contour lines and zoom on them*

All the methods defined here were applied to the sound board and the back of our two violins. All results can be found in the next chapter.

Chapter 6

Results

This final chapter will present all the results we obtained throughout our characteristic points analysis. We will first present the Cuypers 2833, corresponding to the current dimensions of the violins, then the Hofmans 2846 in order to identify the reshaping anomalies. This order runs counter to the chronology but allows the 'ideal' plots to be clearly identified first, and then to show those resulting from alterations. We will then display a 3D version of the presented graphs, in order to more easily relate the 2D plots to the violin itself and allow a better visualisation of the results. Eventually, we will establish a comparison between the recut and the non recut instrument. For most of the graphs, we have first shown a raw result returned by the functions described in the last chapter, and then a filtered and spline approximated result. Most of the filtering was done numerically (height outliers, splines) but to get a good result, some remaining points had to be deleted manually. The interest of manual filtering is to avoid a bad approximation of the splines due to a single misplaced point, as it can be seen in Figure 6.1. Finally, all spline approximations have been made with a smoothness parameter s which allows to influence the regularity of the approximation[24]. However, as raw data differ from one case to another, we could not automate the selection of s and we therefore chose it manually.

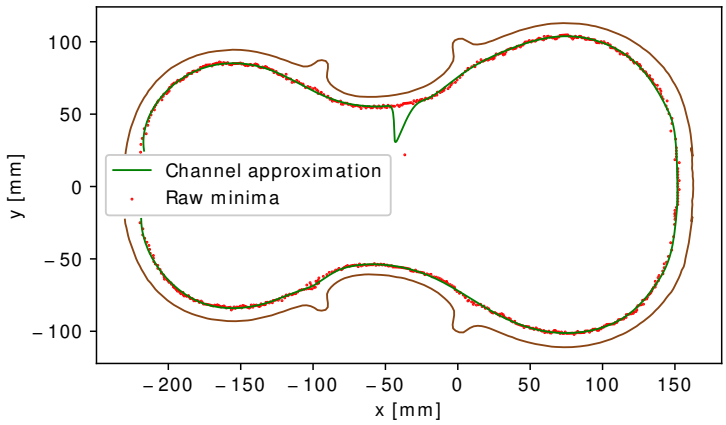
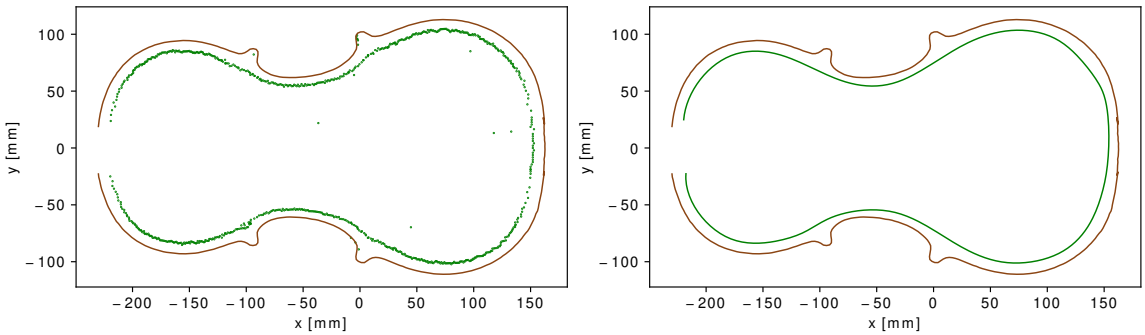


FIG. 6.1 – *Impact of a single outlier on the spline approximation*

24. More on this parameter s in [18].

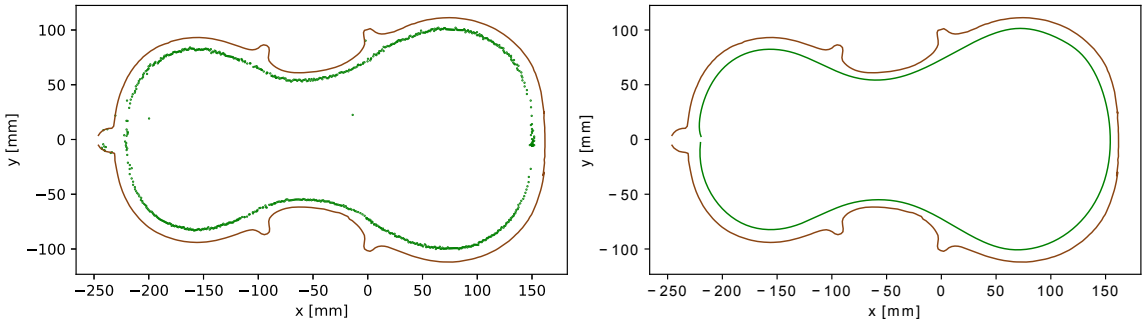
6.1 Cuypers' viola

6.1.1 Channel



(a) *Raw minima* (b) *Channel approximation*

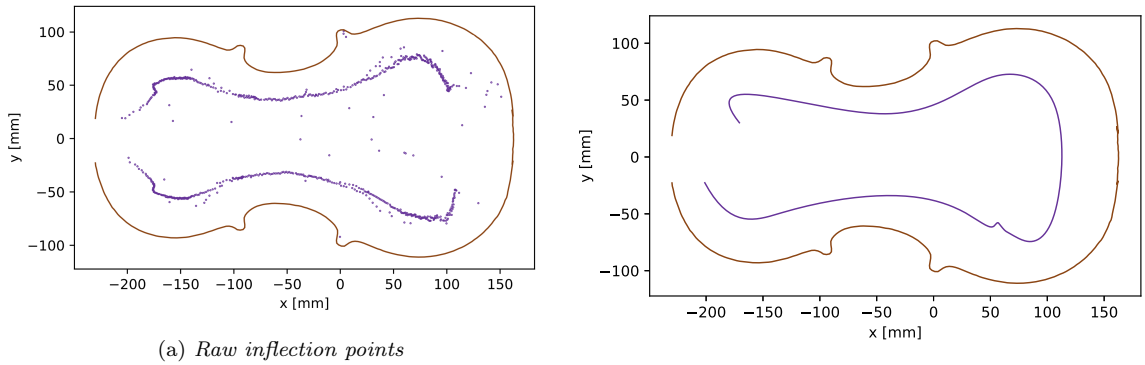
FIG. 6.2 – *Sound board*



(a) *Raw minima* (b) *Channel approximation*

FIG. 6.3 – *Back*

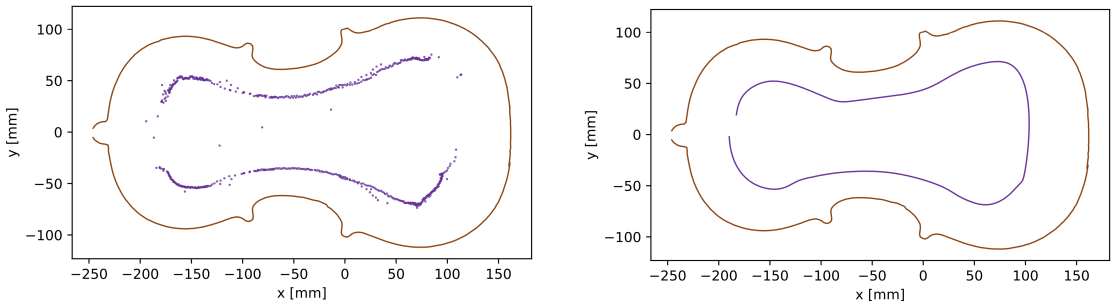
6.1.2 Inflection points path



(a) *Raw inflection points*

(b) *Path approximation*

FIG. 6.4 – *Sound board*

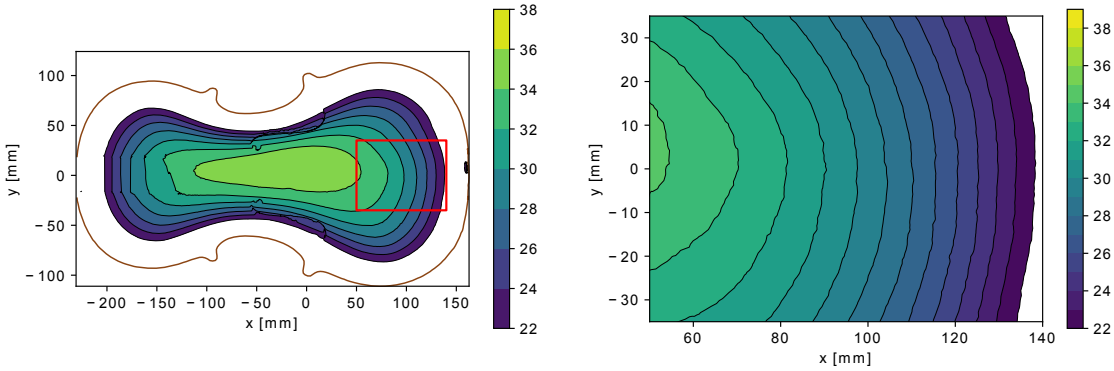


(a) *Raw inflection points*

(b) *Path approximation*

FIG. 6.5 – *Back*

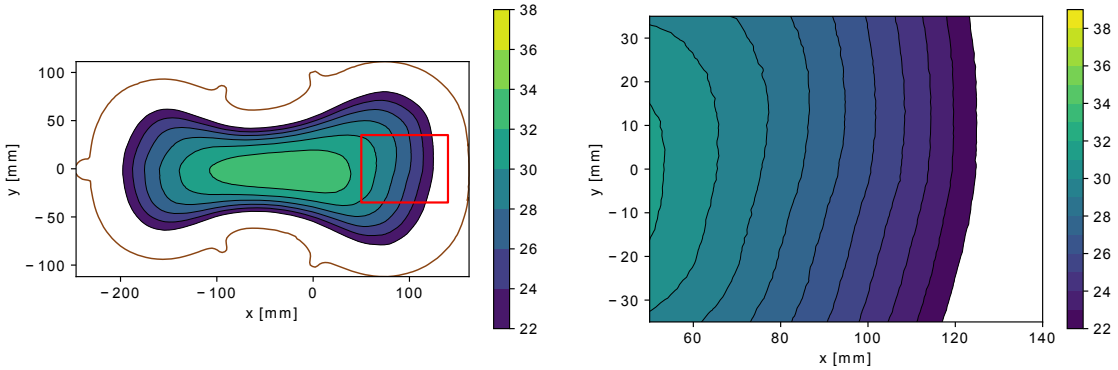
6.1.3 Contour lines



(a) *Contour lines*

(b) *Zoom and refinement*

FIG. 6.6 – *Sound board*



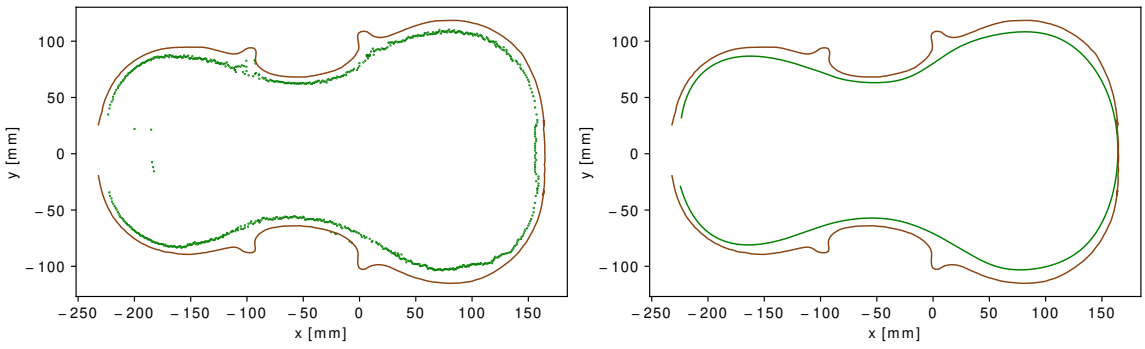
(a) *Contour lines* (b) *Zoom and refinement*

FIG. 6.7 – *Back*

These graphs illustrate the different elements of non recut violins described in Chapter 1. Indeed, the channel remains at an almost constant distance from the edge along the entire circumference. The path of the inflection points is defined a little less precisely, but we observe that the curves have nice roundness that follows the curvy ends of the sound board. Finally, the contour lines are, as expected, rounded and show no signs of abrupt change in sharpness.

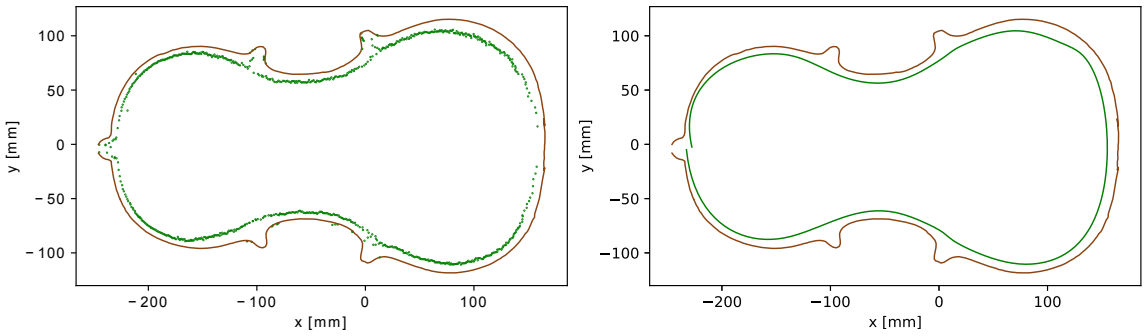
6.2 Hofmans' viola

6.2.1 Channel



(a) *Raw minima* (b) *Channel approximation*

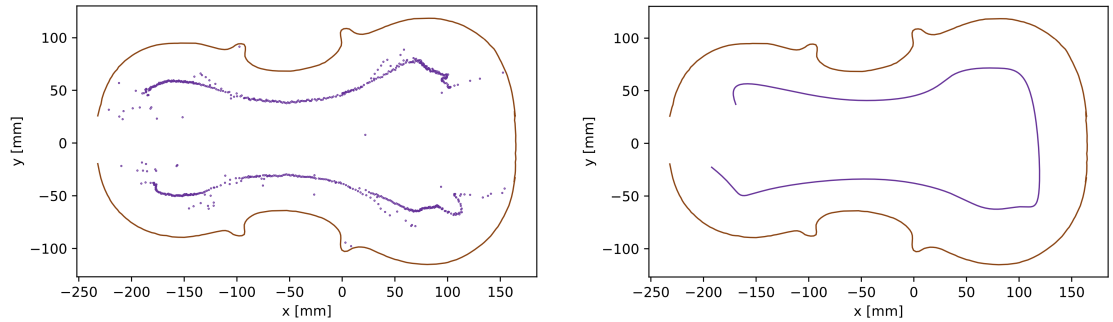
FIG. 6.8 – *Sound board*



(a) *Raw minima* (b) *Channel approximation*

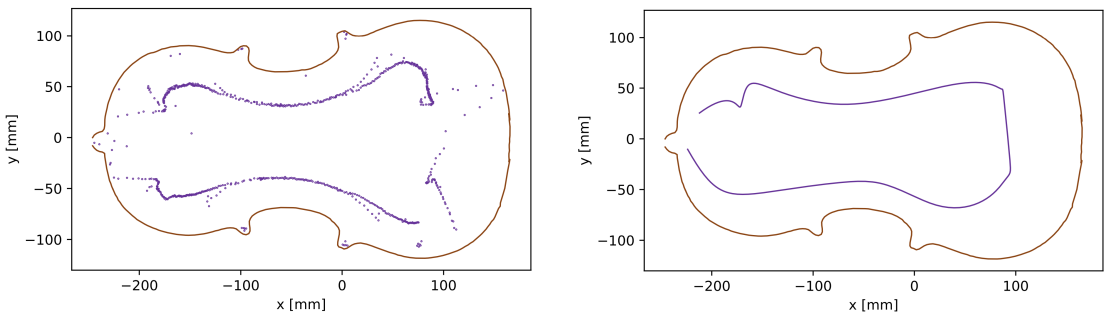
FIG. 6.9 – *Back*

6.2.2 Inflection points path



(a) *Raw inflection points* (b) *Path approximation*

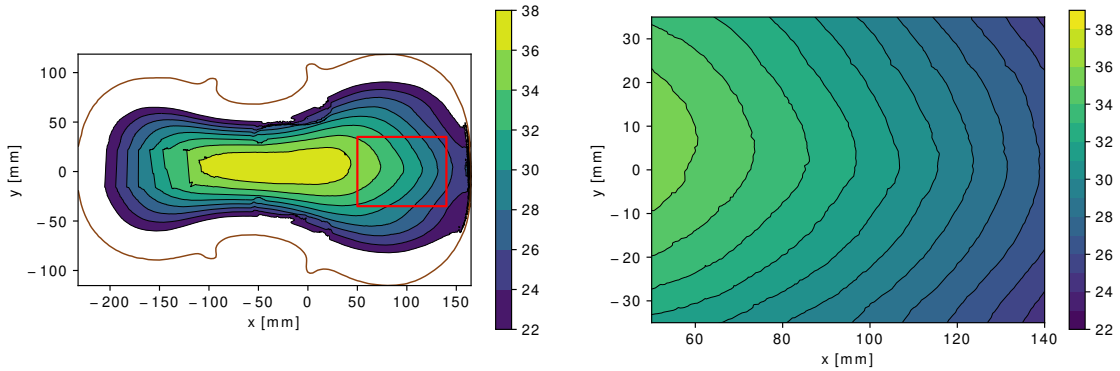
FIG. 6.10 – *Sound board*



(a) *Raw inflection points* (b) *Path approximation*

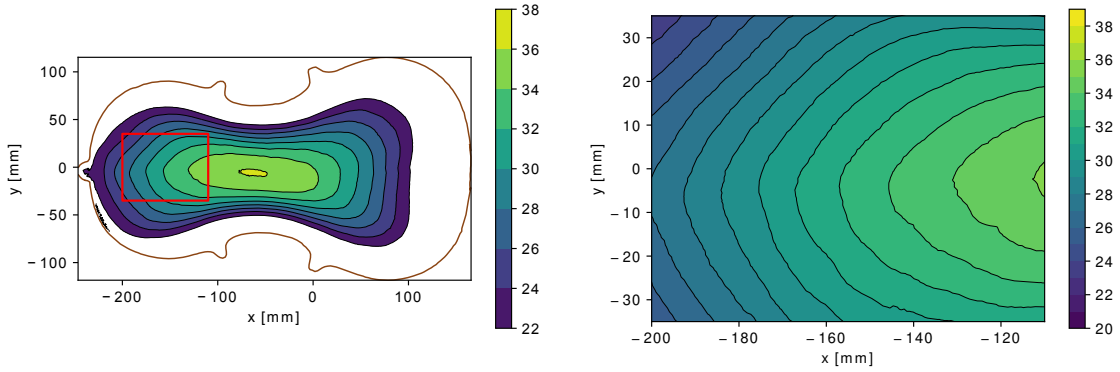
FIG. 6.11 – *Back*

6.2.3 Contour lines



(a) *Contour lines* (b) *Zoom and refinement*

FIG. 6.12 – *Sound board*



(a) *Contour lines* (b) *Zoom and refinement*

FIG. 6.13 – *Back*

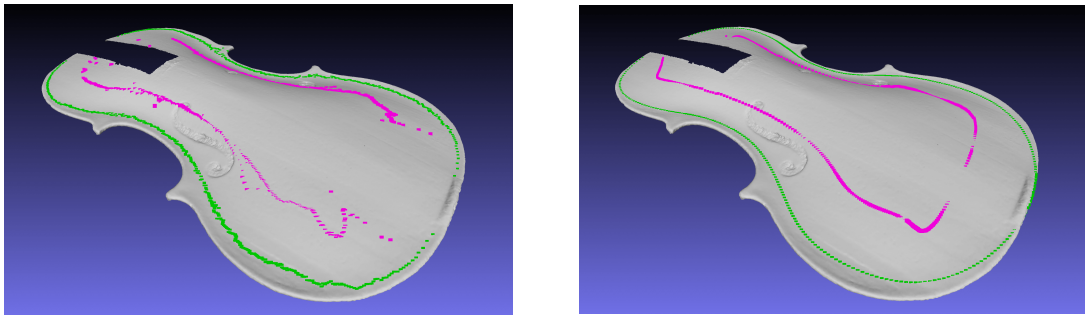
We can observe the impact of reshaping on the different graphs shown above. The channel is closer to the edges and merges with the bottom of the sound board while the path of the inflection points is steeper than on a non recut violin and adopts a less curved behaviour. Finally, we see that the contour lines are indeed sharper on a recut violin. However, this result on violas is completely unprecedented. Indeed, as mentioned in Chapter 1, the few existing pieces of evidence suggest that the removal of a slice of wood was done on larger instruments such as cellos, but without absolute certainty. Prof. A.-E. Ceulemans has proposed to study contour lines on violas on a hypothetical basis rather than in comparison with other works or testimonies. However, the results are suggestive and let us think that the removal of a slice of wood from the sound board is a more common practice than musicologists had imagined.

We see in Figures 6.8b and 6.9b that the spline approximations of the channel differ between the sound board and the back. This shows that it is very interesting to keep the raw results to relativise the quality of the spline approximations. Indeed, the raw minima

in Figure 6.9a suggest that the back channel should be closer to the edge than shown in Figure 6.9b, especially since there is no saddle on the violin back that could distort the computation. Another strange finding should be mentioned. We see that the contour lines in Figure 6.13a are sharp on one side but very flat on the other. We therefore assume that the luthier who standardised the Hofmans 2846 only partially planed its back. To better understand and enlarge our analysis, it is also important to visualise our results in three dimensions.

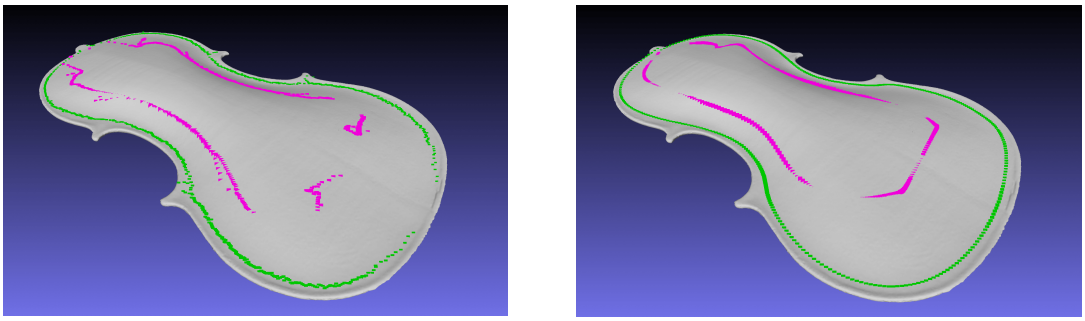
6.3 3D visualisation

The spline approximations of the channel and path presented above were performed in two dimensions. Thus, the spline points illustrated are expressed in (x_{fit},y_{fit}) coordinates. To assign them a z_{fit} component, we have used the FLANN algorithm described in Chapter 4 to find the (x,y,z) point of the initial cloud such that the distance between the (x,y) and (x_{fit},y_{fit}) coordinates is the smallest. Finally, we have assigned the z coordinate of the points returned by FLANN to each spline point (x_{fit},y_{fit}). The following figures illustrate the channel and path together on each surface studied. Once again, we show the raw results first and then the filtered. There is no additional comment compared to the 2D plots, except that the 3D graphs may allow a better visualisation of the results, such as the sound board channel that runs in front of the saddle for a non recut violin and behind it for a recut violin.



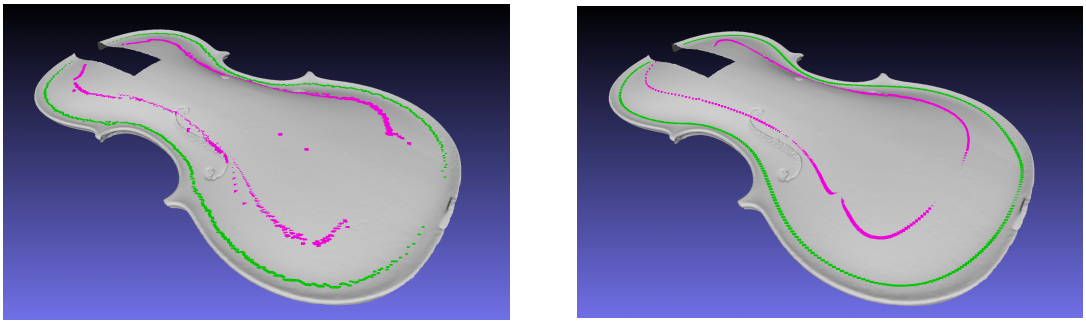
(a) *Raw* (b) *Filtered*

FIG. 6.14 – *Hofmans 2846 sound board : channel (green) and inflection path (magenta)*



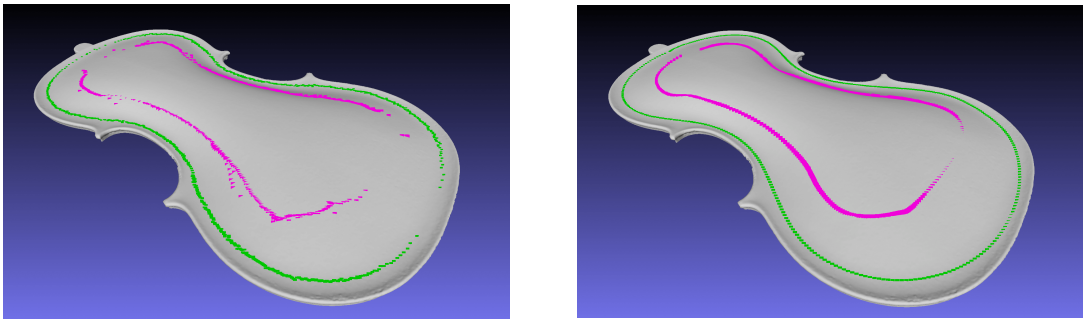
(a) *Raw* (b) *Filtered*

FIG. 6.15 – *Hofmans 2846 back : channel (green) and inflection path (magenta)*



(a) *Raw* (b) *Filtered*

FIG. 6.16 – *Cuypers 2833 sound board : channel (green) and inflection path (magenta)*

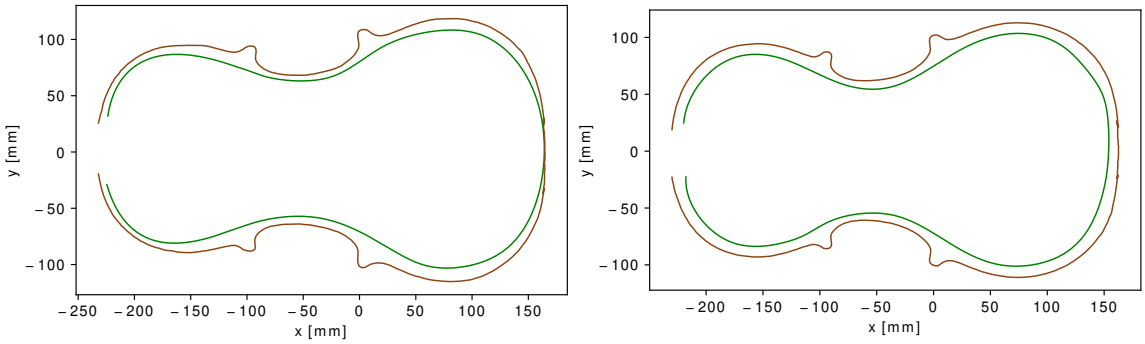


(a) *Raw* (b) *Filtered*

FIG. 6.17 – *Cuypers 2833 back : channel (green) and inflection path (magenta)*

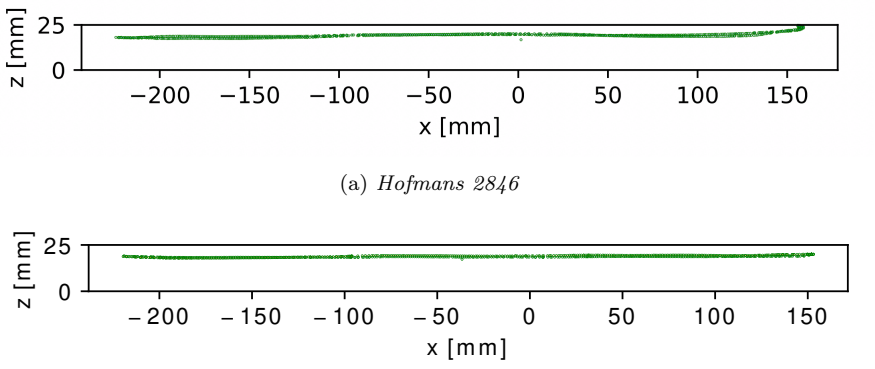
6.4 Comparison between recut and non recut instruments

Through all these plots, we can see that we have been able to find the typical characteristics of a recut or non recut instrument, as explained in Chapter 1. Indeed, the shape of the channel, the layout of the inflection points path and the contour lines are really distinct between the Hofmans 2846 and the Cuypers 2833. We will establish a final comparison for each feature. First of all, we see in Figure 6.18 that the channel of a recut violin tends to shorten at the edges, or even disappear altogether. This is not the case for an intact instrument. Moreover, as we noted in the previous chapter, the channel of a recut instrument tends to raise at the end of the sound board. The comparison between the two channels can be seen in Figure 6.19. Secondly, if we pay attention to the inflection points, we realise that when the instrument has not been recut, they adopt a more curved path which follows the rounded shape of the contours, while they become a little stiffer when it has been modified, as in Figure 6.20. Finally, as hypothetically supposed in Figure 1.9b, the contour lines are sharper on a recut instrument and rounder on a non recut instrument. Again, the difference between the two instruments is clear and can be seen in Figure 6.21. As the comparison was made for only two instruments, it is somewhat simplistic to generalise our results to all violins, whether or not they were reshaped. However, they invite further research on a larger corpus of instruments.



(a) *Hofmans 2846* (b) *Cuypers 2833*

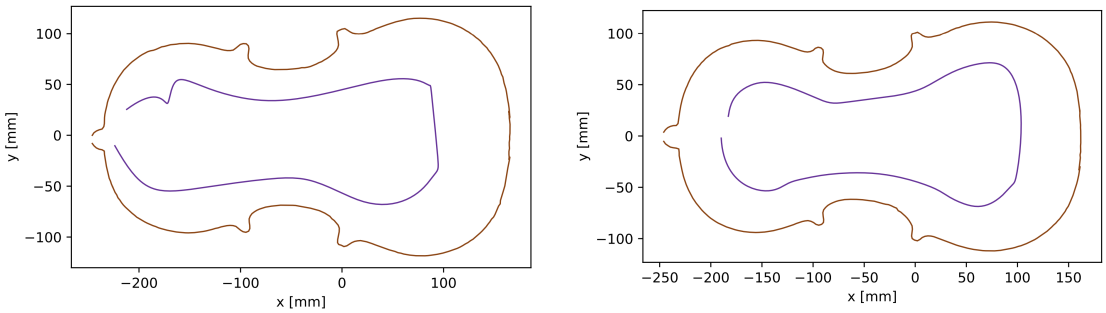
FIG. 6.18 – *Comparison of the sound board channel for both violins*



(a) *Hofmans 2846*

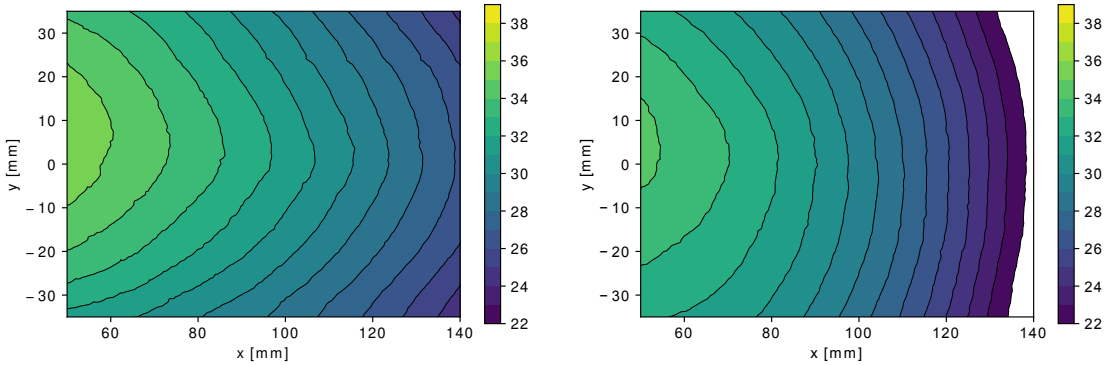
(b) *Cuypers 2833*

FIG. 6.19 – *Profile view of the sound board channel for both violins*



(a) *Hofmans 2846* (b) *Cuypers 2833*

FIG. 6.20 – *Comparison of the back inflection points path for both violins*



(a) *Hofmans 2846* (b) *Cuypers 2833*

FIG. 6.21 – *Comparison of the sound board contour lines for both violins*

Conclusion

The morphology of today's violin differs greatly from that of the first instruments of the late 16th century. Indeed, in order to meet the standards suggested by famous orchestras and conservatories, many ancient violins have been recut. It is important for musicologists and organologists to be able to quantify the alterations these instruments have undergone. With this in mind, the Musical Instruments Museum, and more precisely Prof. A.-E. Ceulemans, launched the design of a digital analysis tool as a subject for an engineering thesis. It is thus in a multi-disciplinary research process that this work was immersed throughout the year. On the one hand, a discussion with musicologists helped to target the objectives of this thesis. On the other hand, thanks to engineers and people experienced with photogrammetry, we were able to achieve our goals.

We involved many different software packages in our process. This diverse use has allowed us to benefit from their built-in functions to greatly facilitate our task. Indeed, we can think of the violins orientation which caused a lot of troubles in the previous thesis, whereas here, it was automatically set in MeshLab. Moreover, as we proved that the PCA alignment was optimal, we drew advantages from this optimality to justify some of our algorithms or searching methods.

The disadvantage of an approach with a lot of software is that there is a long pre-processing phase, but it is nevertheless necessary to derive qualitative results. We can also point out another drawback in our approach. Indeed, although simpler than medical CT scanners, the photo shooting still required professional equipment and expertise. In addition, the license for photogrammetry software such as Agisoft Metashape is not free, unlike Python and MeshLab. Fortunately, as Iona Thys works for the Royal Museums of Art and History of Brussels, of which the MIM is a part, the process remains internal to the museums.

After reconstructing the instruments using photogrammetry, we compared them with the scans that had been taken and saw that a similar analysis to the one made in the previous thesis was feasible, which is good in view of the professional means that had been used. We then highlighted the points of interest from an organological point of view. Even if we cannot conclude in the area where the fingerboard has been removed, the rest of our graphs show that we were able to locate the channel quite precisely on our two violins, which is a very important result for musicologists. The contour lines analysis, which was new compared to the two previous theses, also showed the influence of re-cutting on violins. Our feelings are somewhat mixed about the inflection points results. Unfortunately, as the wood of violins is sensitive to time, humidity, air and many more, the morphology of the sound board or the back may be irregular. From an algorithmic point of view, there is no single type of cut through the mesh and it is therefore difficult to generalise a searching

approach, which moreover involves first and second derivatives. However, their path is still distinct between a recut and a non recut violin and we were able to identify their general appearance. Refinements to the inflection path computation are left for further research, perhaps with a global three-dimensional approach avoiding the need for cuts.

We are finally satisfied to have validated our photogrammetric approach. Despite the slight flaws introduced, the results returned are still sufficiently accurate for musicologists and organologists (we recall that we have worked with a millimetre accuracy throughout this thesis). This means that we could extend our approach to many more instruments. In the long run, we could even try to establish a classification of a given instrument using a machine learning approach. We could also try to estimate the dimensions of the recut parts of an instrument and thus its original dimensions. However, it would be necessary to create a substantial database from a large corpus of violins.

References

[1] Ceulemans A.-E., *De la vièle médiévale au violon du XVIIe siècle. Etude terminologique, iconographique et théorique*,Tours, Centre d'études supérieures de la Renaissance - Turnhout. Brepols, 2011

[2] Moens K. *Les voix médianes dans l'orchestre français sous le règne de Louis XIV*, L'orchestre à cordes sous Louis XIV. Instruments, répertoires, singularités, dir. J. Duron - F. Gétreau, Paris, 2015, p. 119-138

[3] Cozio di Salabue I. A., *Carteggio*, ed. by Bacchetta R. and Iviglia G., Milano, Cordani, 1950, p. 114-115

[4] Tolbecque A., *L'art du luthier*, Niort, L'Auteur, 1903, p. 244-245 (retrievable at `https://archive.org/details/lartduluthier00tolbgoog`)

[5] Stowell R., *Violin Technique and Performance Practice in the Late Eighteenth and Early Nineteenth Centuries*, Cambridge, Cambridge University Press, 1990, p. 27

[6] Sibire S.-A., *La Chélonomie, ou, Le parfait luthier*, Brussels, Weissenbruch, 1823, p. 128-129 (retrievable at `https://www.luthiers-mirecourt.com/sibire_la_chelonomie.htm`)

[7] Herzog M. *The Quinton and other Viols with Violin Traits*, Volume I, Ph.D. Bar-Ilan University, 2003, p. 55 (retrievable at `https://www.academia.edu/35122782/The_Quinton_and_other_Viols_with_Violin_Traits_Ph_D_Thesis_Volume_I`)

[8] Romberg B., *Méthode de violoncelle, adoptée par le directeur du Conservatoire royal de Paris, à l'usage des classes de cet établissement*, Paris, H. Lemoine, 1840, p. 6 (retrievable at `https://gallica.bnf.fr/ark:/12148/bpt6k9633819w/f19.item`)

[9] Houssay A., *Cordes filées et violons en Italie au XVIIe siècle: Quelques cas d'instruments crémonais recoupés*, in *L'orchestre à cordes sous Louis XIV. Instruments, répertoires, singularités*, dir. J. Duron – F. Gétreau, Paris, Vrin, 2015, p. 139-162

[10] Motte L., *Conception d'un outil mathematique/informatique pour la classification d'instruments a archet*, Master thesis, UCL/EPL, 2017, prom. P. Fisette and A.-E. Ceulemans

[11] Lothaire R., *Characterization of violins: a digital tool at the service of organology*, Master thesis, UCL/EPL, 2019, prom. P. Fisette, F. Glineur and A.-E. Ceulemans

[12] Paul A. Yushkevich, Joseph Piven, Heather Cody Hazlett, Rachel Gimpel Smith, Sean Ho, James C. Gee, and Guido Gerig. *User-guided 3D active contour segmentation of anatomical structures: Significantly improved efficiency and reliability.*Neuroimage. 2006 Jul 1; 31(3):1116-28.

[13] Medixant. RadiAnt DICOM Viewer [Software]. Version 2020.2. Jul 19, 2020. URL: https://www.radiantviewer.com

[14] Youtube channel of Mister P. MeshLab Tutorials : `https://www.youtube.com/channel/UC7OCKZQPj_ZAJ0Osrm6TyTg`

[15] Unknown author, Plyfile Github library, `https://github.com/dranjan/python-plyfile`

[16] Rebetez J. (MIT), Meshcut Github library, https://github.com/julienr/meshcut

[17] Muja M., Lowe D. G., Google Inc (Rae J.), FLANN Github library, https://github.com/flann-lib/flann

[18] *Scipy.interpolate* library, https://docs.scipy.org/doc/scipy/reference/interpolate.html

[19] Spline Wikipedia page, https://fr.wikipedia.org/wiki/Spline#Spline_de_lissage

Figures references

All the figures in this thesis come from our own simulations and computations, except :

- Figure 1: From K. Moens in [2]
- Figure 1.1: https://collectionsdumusee.philharmoniedeparis.fr/doc/MUSEE/0156410
- Figure 1.2: https://www.apollium.fr/catalogue/vente_14_musicora-2018/lot_195_violon-franais#.YJez-2aA7AN
- Figure 1.3: https://www.medecine-des-arts.com/fr/article/violon-la-lutherie/anatomie-du-violon-moderne.php
- Figure 1.5: From R. Lothaire in [11]
- Figure 1.6: From I. Thys
- Figure 1.9a: https://maestronet.com/forum/uploads/monthly_12_2008/post-25136-1230652331.jpg, originally from Möckel O., *Die Kunst des Geigenbaues*, Leipzig, Voigt, 1930, p. 144
- Figure 1.9b: Left schema from https://www.platetuning.org/Violin_back_arching_2-_Sergei_Mugatov.jpg, right schema from A.-E. Ceulemans
- Figures 1.10 and 1.11: https://www.carmentis.be/eMP/eMuseumPlus
- Figures 2.1, 2.2 and 2.3a: From L. Motte in [10]
- Figures 2.4, 2.5 and 2.6: From R. Lothaire in [11]
- Figure 3.1: Schemas from A.-E. Ceulemans
- Figures 3.1a and 3.1b: From A.-E. Ceulemans
- Figure 3.3: From S. Le Conte
- Figure 3.4: From A.-E. Ceulemans
- Figures 4.14 and 4.15: Violin drawing from https://clipground.com/violin-drawing-clipart.html

List of figures

1 Recut violin and estimation of its original dimensions. Height of the sound box: now 35.4 *cm* - original c. 38 *cm* 1

1.1 Side view of the violin anatomy 3
1.2 Anatomy of the body, front view of the sound board (left) and back view (right) 4
1.3 Profile of a baroque violin (up) and a modern violin (down) 4
1.4 Different kinds of re-cutting 5
1.5 Cross section of a violin 5
1.6 Channel on the violin sound board 6
1.7 Sagittal section of a recut and non recut violin 6
1.8 Graphical representation of an inflection point (red) 6
1.9 Contour lines 7
1.10 Cuypers Johannes Theodorus, inv. no 2833, The Hague, 1761 8
1.11 Hofmans Matthys IV, inv. no 2846, Antwerp, before 1679 8

2.1 Picture used by L. Motte to recreate the violin in 3D 10
2.2 Approximation of the violin sound board dimensions 10
2.3 Maps of two violin backs from [10] 11
2.4 Cross section of a matrix form violin 12
2.5 Minima channel and inflection points path on the Cuypers 2833 sound board 12
2.6 New way of realising planar cuts, top view of a frontal cut 13

3.1 Two techniques of photogrammetry 16
3.2 Meshes obtained with Autodesk ReCap 16
3.3 Targets helping the reconstruction software 17
3.4 Light tent 18
3.5 Photogrammetric process 18
3.6 3D models of both violins 19
3.7 Comparison of the point clouds of the two shootings for the Hofmans 2846 sound board 19
3.8 General process of the thesis 20

4.1 Fingerboard distinct or merged with the body 22
4.2 Cuypers 2833 repair 22
4.3 Different views of the reference frame 23
4.4 Before and after the PCA alignment 23
4.5 Alignment of the bounding box and the frame after the PCA 24
4.6 Other possible reference frames by moving the y axis on the x axis 24
4.7 Comparison of the measures in MeshLab and RadiAnt Viewer 25

4.8 Cuypers 2833 cross section (top left), sagittal section (top right) and frontal section (bottom right) in ITK-SNAP . . . 26
4.9 2D evolution of the algorithm on cross sections . . . 27
4.10 3D evolution of the algorithm . . . 27
4.11 Swelling effect to be avoided . . . 27
4.12 Different thresholds . . . 28
4.13 DICOM meshes of Cuypers 2833 (top) and Hofmans 2846 (bottom) . . . 28
4.14 Representation of both meshes in the frame of reference . . . 29
4.15 Representation of both meshes in their own frame . . . 30
4.16 FLANN minimisation for each individual parameter . . . 32
4.17 Distances distribution representations (with K) . . . 34
4.18 Filtered distributions . . . 35

5.1 Cross sections in MeshLab . . . 38
5.2 Isolated sound board and back . . . 39
5.3 Top view of sound board and back . . . 39
5.4 General Python process of the sound board coordinates isolation . . . 40
5.5 Discrete contour of the Hofmans 2846 soundboard . . . 41
5.6 Intuitive and mathematical representations of the sound board bottom . . . 42
5.7 Discrete and spline approximation of the Hofmans 2846 sound board . . . 43
5.8 Planar cut in both frames . . . 43
5.9 Effect of the averaging on the non defined points . . . 45
5.10 Upper part of the sound board without overhanging edges . . . 45
5.11 Computing minima process . . . 46
5.12 Channel on Hofmans 2846 sound board . . . 46
5.13 Profile view of the channel before and after filtering . . . 47
5.14 Profile view of the filtered Cuypers 2833 sound board channel . . . 47
5.15 Filtered channel on Hofmans 2846 sound board . . . 48
5.16 Impact of the saddle on the minima location . . . 48
5.17 Channel approximation with or without considering the bottom raw minima 49
5.18 Different outputs of Algorithm 6 . . . 50
5.19 Inflection points location . . . 51
5.20 Contour lines . . . 52
5.21 Relevant contour lines and zoom on them . . . 52

6.1 Impact of a single outlier on the spline approximation . . . 53
6.2 Sound board . . . 54
6.3 Back . . . 54
6.4 Sound board . . . 55
6.5 Back . . . 55
6.6 Sound board . . . 55
6.7 Back . . . 56
6.8 Sound board . . . 56
6.9 Back . . . 57
6.10 Sound board . . . 57
6.11 Back . . . 57
6.12 Sound board . . . 58
6.13 Back . . . 58
6.14 Hofmans 2846 sound board : channel (green) and inflection path (magenta) . 59
6.15 Hofmans 2846 back : channel (green) and inflection path (magenta) . . . 59

6.16 Cuypers 2833 sound board : channel (green) and inflection path (magenta) . 60
6.17 Cuypers 2833 back : channel (green) and inflection path (magenta) 60
6.18 Comparison of the sound board channel for both violins 61
6.19 Profile view of the sound board channel for both violins 61
6.20 Comparison of the back inflection points path for both violins 61
6.21 Comparison of the sound board contour lines for both violins 62

UNIVERSITÉ CATHOLIQUE DE LOUVAIN
École polytechnique de Louvain
Rue Archimède, 1 bte L6.11.01, 1348 Louvain-la-Neuve, Belgique | **www.uclouvain.be/epl**